Electronic Supplementary Information (ESI) for 'Night-time oxidation of surfactants at the air–water interface: effects of chain length, head group and saturation.'

Federica Sebastiani,[a,b] Richard A. Campbell,[b] Kunal Rastogi[a] and Christian Pfrang.[a*]

[a] Department of Chemistry, University of Reading, P.O. Box 224, RG6 6AD, Reading, UK
[b] Institut Laue-Langevin, 71 avenue des Martyrs, CS20156, 38042 Grenoble Cedex 9, France
* corresponding author: c.pfrang@reading.ac.uk

1. Materials and Preliminary Characterisation

Table 1: List of the organic surfactants used for the experiments including molecular weight (MW) and scattering length (SL). * indicates the custom-deuterated molecules provided by the Oxford Deuteration Facility.

Molecule	Chemical formula	MW / g mol^{-1}	SL / fm
d_{33}MO*	$CD_3(CD_2)_7CD=CD(CD_2)_7CO_2CH_3$	329.69	346.80
d_{34}OA	$CD_3(CD_2)_7CD=CD(CD_2)_7CO_2D$	316.67	358.05
d_{14}POA*	$CH_3(CH_2)_5CH=CH(CD_2)_7CO_2H$	268.49	151.49
d_{35}SA	$CD_3(CD_2)_{16} CO_2H$	319.69	360.98

The thermodynamic properties of the organic monolayers have been investigated by measuring the pressure isotherm as a function of the surface area on a Langmuir trough.[1] The in plane structure of the monolayer was monitored with Brewster angle microscopy (BAM) imaging while compressing the film to record the isotherm. Those two techniques used in combination allowed the characterization of the phase behavior of the single component monolayer, revealing the phase transition regions and the optical properties, such as anisotropy. OA and MO reach a plateau and they form lenses on top of the isotropic monolayer, while POA does not reach a clear plateau and the monolayer remains isotropic all over the compression. The surface pressure reached at the plateau is similar for OA and POA, while MO reaches a much lower pressure. This suggests a lower chain ordering for MO due to the poor hydrophilicity of the head group compared to the parent fatty acid, OA. SA shows in plane structure already at 0 mNm^{-1} and further compression leads to solid-like structures.
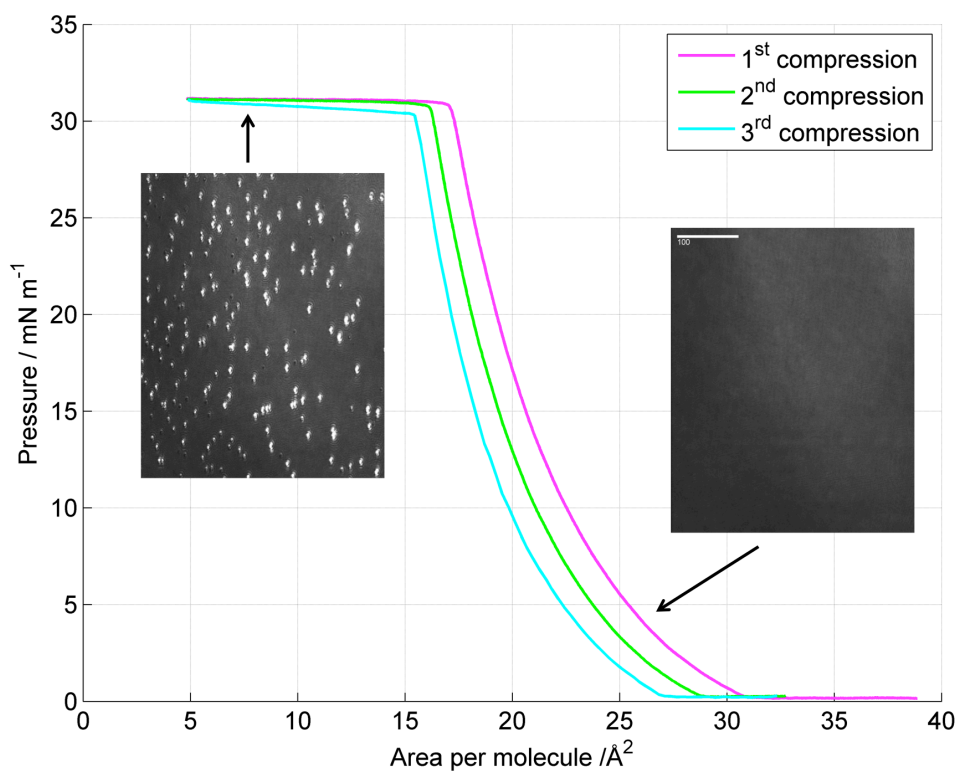
2   **Figure 1.** Surface pressure isotherm of *h*MO at 25 °C on a water subphase with the
3   corresponding BAM images of the monolayer recorded at two pressures: 3 mNm^{-1}: the layer
4   is isotropic; and 16.2 mNm^{-1}: the layer is collapsed. The white bar corresponds to 100 μm.
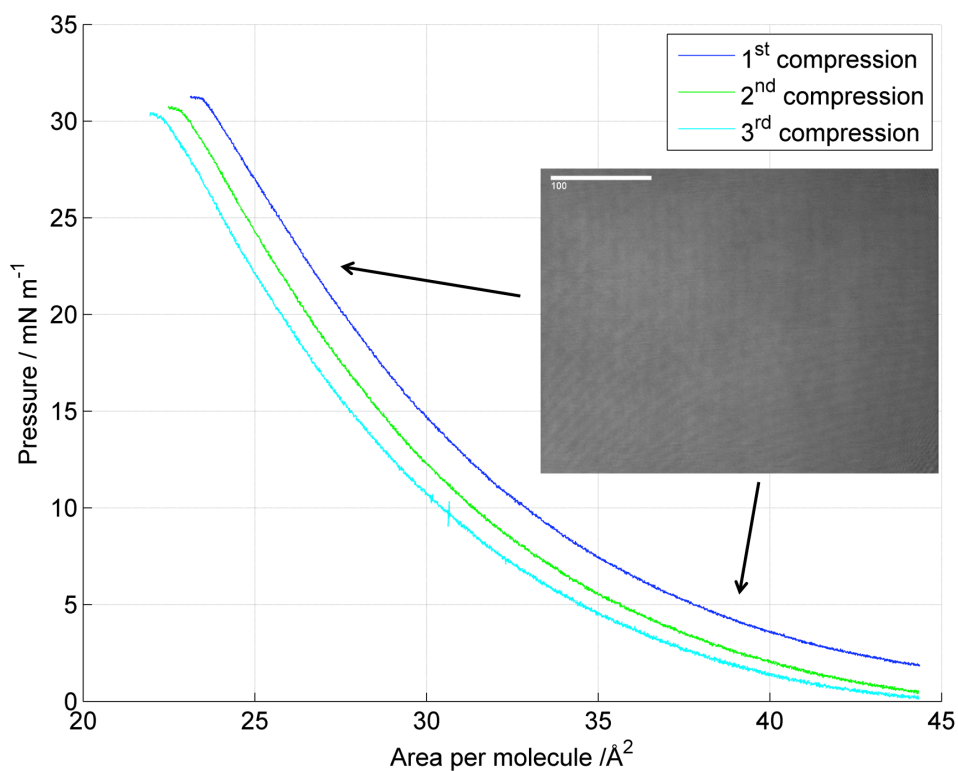
6   **Figure 2.** Surface pressure isotherm of *h*POA at 25 °C on a water subphase with the
7   corresponding BAM image recorded at low pressure. The layer is isotropic at all pressures.
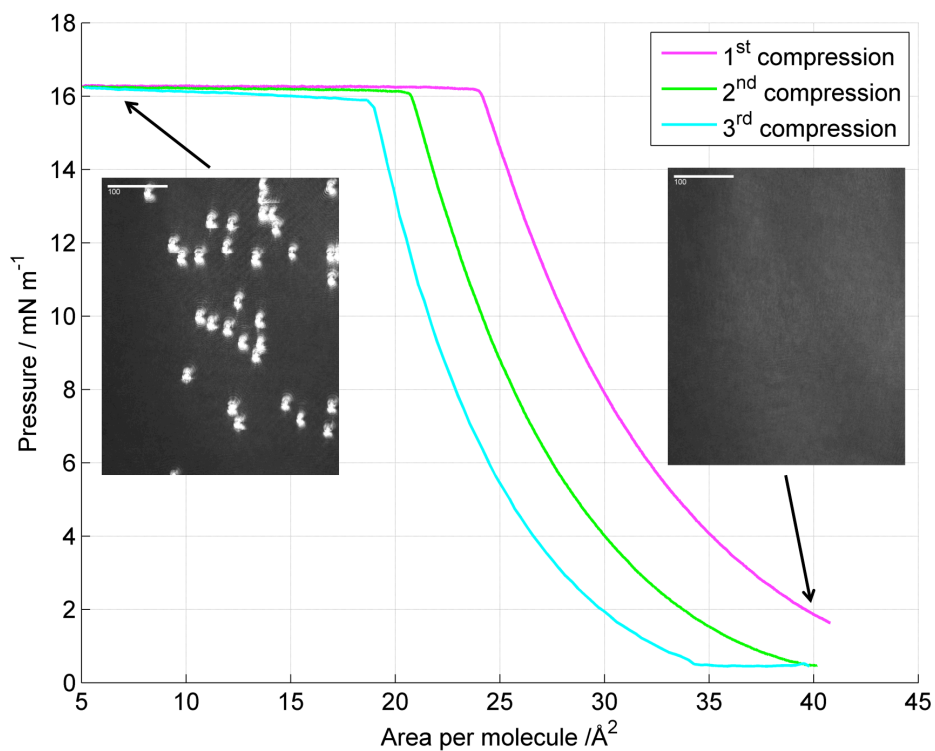
2 **Figure 3.** Surface pressure isotherm of *h*OA at 25 °C on a water subphase with the
3 corresponding BAM images recorded at two pressures: 3 mNm^{-1}: the layer is isotropic; and
4 32 mNm^{-1}: the layer is collapsed. The white bar corresponds to 100 μm.
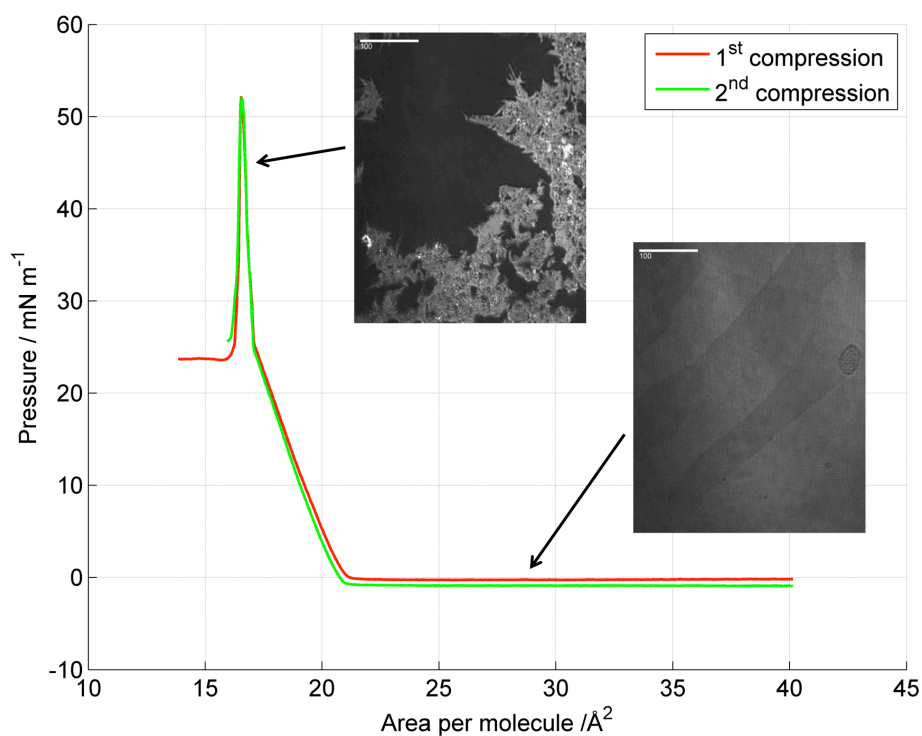
7 **Figure 4.** Surface pressure isotherm of *h*SA at 25 °C on a water subphase with corresponding
8 BAM images recorded at two pressures: 0 mNm^{-1}: domains can be distinguished; and 45
9 mNm^{-1}: organised structures are formed. The white bar corresponds to 100 μm.

2. Gas Flow System

Fig. 5 shows a sketch of the gas flow system. For the production of NO_3, the O_2 flow was kept at 1.2 dm^3 min^{-1} and the flow rate of NO_2 ranged between 0.06 to 0.36 dm^3 cm^{-1}. The mixing bulb has a volume of 5 dm^3, and the inlet part is made of a glass cylinder with 21 small holes on the surface, which enhances mixing of the components. The residence time in the mixing bulb ranges from 2 to 4 minutes, which is long enough to establish equilibrium within the products. The concentration of NO_3 is tuned by changing the NO_2 flow rate and hence its concentration. $[NO_2]$ is always in large excess of $[O_3]$ to ensure that all the ozone is consumed before the gas flow reaches the organic film.
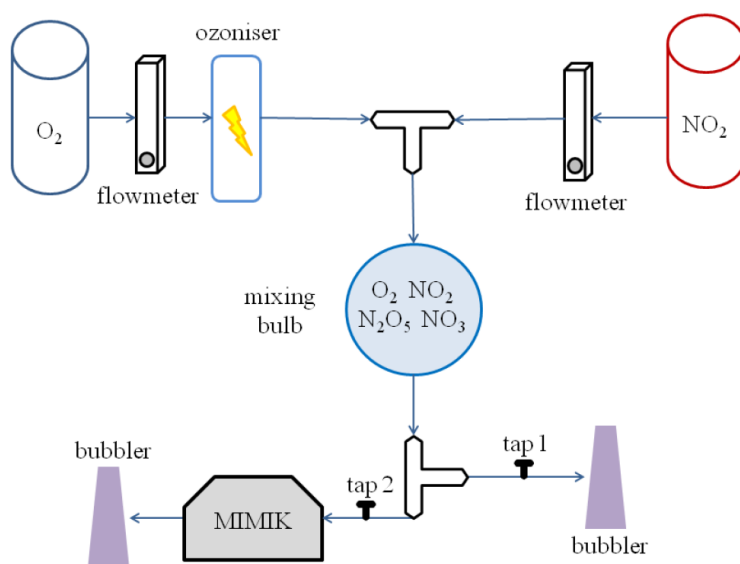
Figure 5. Schematic of the gas flow system. The arrow represents the direction of the flow. On the top left side the ozone is produced, then it mixes with NO_2 just before the inlet of the mixing bulb. From the mixing bulb the mixture can directly go to an exhaust bubbler or pass through the reaction chamber.

The tubing is made from Chemfluor® (PTFE), with an outer diameter of 1/4 inch and an inner diameter of 1/8 inch; this material has been chosen for its high chemical resistance. A digital flow meter (Model MV-302, MASS–VIEW, Bronkhorst) has been used for the control of the O_2 flow. For the NO_2 a ball flow meter (Cole Parmer) resistant to NO_2 corrosion has been used. All the connectors used were made of Teflon or stainless steel to ensure chemical resistance.

3. Reaction Model and Spectroscopic Measurements

We produced NO_3 by reacting varying concentrations of NO_2 with a given ozone concentration. $[NO_3]$ could not be measured directly, but we calculated $[NO_3]$ from spectroscopic measurements of $[NO_2]$ and $[N_2O_5]$.

3.1 Reaction model

The reactions considered for description of the *in situ* production of NO_3 are shown below:

$$NO_2 + O_3 \rightarrow NO_3 + O_2 \ (k_1) \tag{R1}$$

$$NO_2 + NO_3 + M \rightarrow N_2O_5 + M \ (k_2) \tag{R2}$$

$$N_2O_5 + M \rightarrow NO_3 + NO_2 + M \ (k_3) \tag{R3}$$
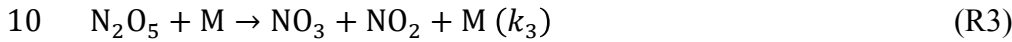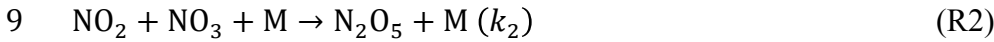
In order to simulate the reactions, the concentrations of the gas-phase species are calculated as a function of time relying on published rate coefficients evaluated in the review ``Chemical kinetics and photochemical data for use in atmospheric studies (evaluation No. 17)" by Sander *et al.*[2] (the type of reaction and the ambient conditions, *i.e.* temperature and pressure are appropriately taken into account; the conditions chosen for the calculation are 298.15 K (25 °C) and atmospheric pressure, 1 atm). For further details on the following Eqs 1–7 see Seinfeld and Pandis, 2006.[3] The first reaction is a bimolecular reaction and the rate coefficient is described as:

$$k_1(T) = Ae^{-(E/RT)} \tag{1}$$

$A = 1.2 \times 10^{-13}$ cm^3 molecule^{-1} s^{-1} and $E/R = 2450$ K,[2] those values are valid for temperature ranging from 230 to 360 K. Reaction R2 is a termolecular reaction and the rate coefficient, $k_2(T,[M])$, is estimated using the expression described by Troe[4]. The concentration of the third body, $[M]$, is related directly to the pressure, in the atmosphere M is the sum of N_2 and O_2 and approximating to ideal gas we can use $[M] = N_{Av}/V_{mole} = 2.46 \times 10^{19}$ molecule cm^{-3}.

$$k_2(T,[M]) = \frac{k_{0,2}(T)[M]}{1+(k_{0,2}(T)[M]/k_{\infty,2}(T))} 0.6^{\left[1+\left(\log(k_{0,2}(T)[M]/k_{\infty,2}(T))\right)^2\right]^{-1}} \tag{2}$$

where $k_{0,2}(T)$ is the low-pressure limiting value for $k_2(T,[M])$ and the dependence on temperature is expressed as:[3,4]

$$k_{0,2}(T) = k_{0,2}^{300} \left(\frac{T}{300}\right)^{-n} \tag{3}$$

1 where $k_{0,2}^{300} = 2 \times 10^{-30}$ cm^6 molecule^{-2} s^{-1} is the value at 300 K and $n = 4.4$ (valid for T in the

2 range 200 – 300 K), both values were taken from Ref.[2]. The $k_{\infty,2}(T)$ is the high-pressure limit

3 value for $k_2(T,[M])$ and the dependence on temperature is expressed as:[3,4]

4 $$k_{\infty,2}(T) = k_{\infty,2}^{300} \left(\frac{T}{300}\right)^{-m} \qquad (4)$$

6 where $k_{\infty,2}^{300} = 1.4 \times 10^{-12}$ cm^3 molecule^{-1} s^{-1} is the value at 300 K and $m = 0.7$ (valid for

7 temperature in the range 200 – 400 K), both values were taken from Sander $et\ al.$[2]

8 Reaction R3 is similar to the previous one,[4] but the calculation of $k_{0,3}$ and $k_{\infty,3}$ is slightly

9 different, see Eqs 6 and 7.

10 $$k_3(T,[M]) = \frac{k_{0,3}(T)[M]}{1+(k_{0,3}(T)[M]/k_{\infty,3}(T))} 0.6^{\left[1+(\log(k_{0,3}(T)[M]/k_{\infty,3}(T)))^2\right]^{-1}} \quad (5)$$

12 The low-pressure limit for $k_3(T,[M])$ is calculated as:

13 $$k_{0,3}(T) = k_{0,3}^{300} \left(\frac{T}{300}\right)^{-p} e^{-L/T} \qquad (6)$$

15 where $k_{0,3}^{300} = 1.3 \times 10^{-3}$ cm^3 molecule^{-1} s^{-1} is the value at 300 K, $L = 11000$ K and $p = 3.5$

16 (valid for temperature ranging from 200 to 400 K), all values stated were taken from Sander

17 $et\ al.$[2] The high-pressure limit for $k_3(T,[M])$ is expressed as:

18 $$k_{\infty,3}(T) = k_{\infty,3}^{300} \left(\frac{T}{300}\right)^{q} e^{-N/T} \qquad (7)$$

20 where $k_{\infty,3}^{300} = 9.7 \times 10^{14}$ cm^3 molecule^{-1} s^{-1} is the value at 300 K, $N = 11080$ K and $q = 0.1$

21 (valid for temperature in the range 200 – 400 K). All the values are taken from Sander $et\ al.$[2]

23 **Table 2.** Estimation of the rate constants for the reactions R1 – R3 in the conditions: $T = 25°C$
24 and pressure 1 atm.

Rate	Value
k_1 (298.15 K)	3.2×10^{-17} cm^3 molecule^{-1} s^{-1}
k_2 (298.15 K)	1.18×10^{-12} cm^3 molecule^{-1} s^{-1}
k_3 (298.15 K)	0.06 s^{-1}

31 Once all the rate coefficients are obtained for the correct conditions (Table 2), the differential

32 equations describing the reactions R1 – R3 (Eqs 8 – 11) can be solved numerically in order to

33 obtain the concentrations as a function of time for the various chemical compounds.

34 $$\frac{d[O_3]}{dt} = -k_1[O_3][NO_2] \qquad (8)$$

1    $\dfrac{d[\text{NO}_2]}{dt} = -k_1[\text{O}_3][\text{NO}_2] - k_2[\text{NO}_2][\text{NO}_3] + k_3[\text{N}_2\text{O}_5]$ (9)

2    $\dfrac{d[\text{N}_2\text{O}_5]}{dt} = k_2[\text{NO}_2][\text{NO}_3] - k_3[\text{N}_2\text{O}_5]$ (10)

3    $\dfrac{d[\text{NO}_3]}{dt} = k_1[\text{O}_3][\text{NO}_2] - k_2[\text{NO}_2][\text{NO}_3] + k_3[\text{N}_2\text{O}_5]$ (11)

5   The system of equations has been implemented in Matlab.[5] The solutions have been

6   computed for several initial $[\text{NO}_2]$ values, corresponding to the gas conditions chosen for the

7   NR and IR experiments. The initial concentration of ozone was fixed to 1.05×10^{14} molecule

8   cm^{-3}. This value was obtained from the calibration of the ozoniser performed with the UV-

9   Vis using a flow rate of 1.2 dm^3 min^{-1}.

10   Figs 6–9 show the concentrations of the various gas species as a function of time and their

11   dependence on the initial NO_2 concentrations.
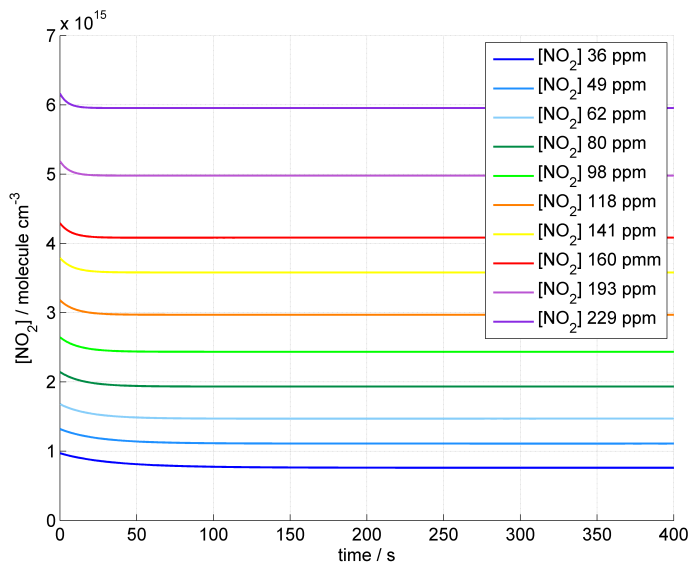
14   **Figure 6.** Time evolution of $[\text{NO}_2]$ calculated from Eqs 8–11 for several initial values of

15    $[\text{NO}_2]$. The initial values of $[\text{NO}_2]$ are reported in the legend.
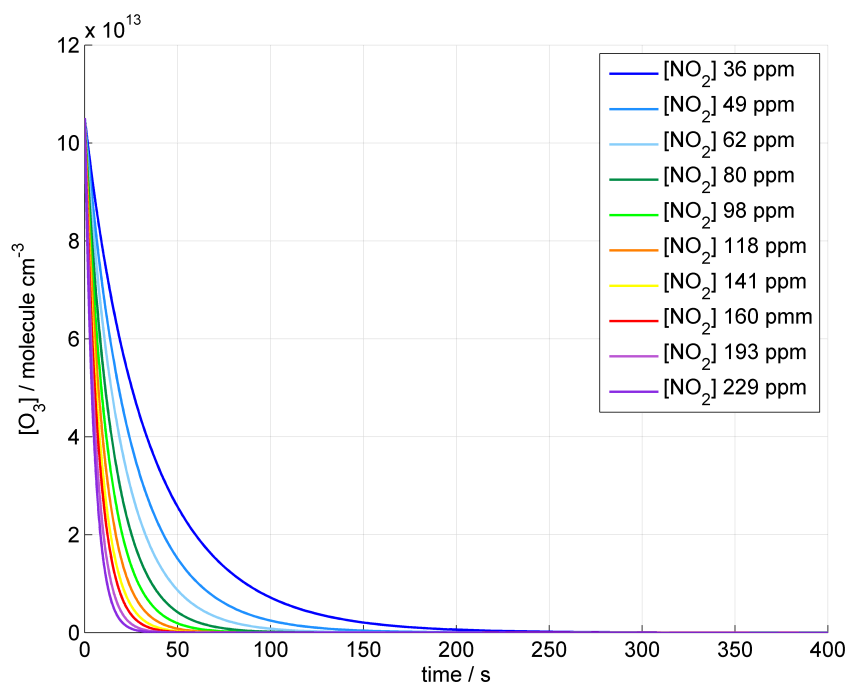
2 **Figure 7.** The consumption of O_3 as a function of $t,$ calculated from Eqs 8–11 as a function of
3 different initial $[NO_2]$ values is displayed.
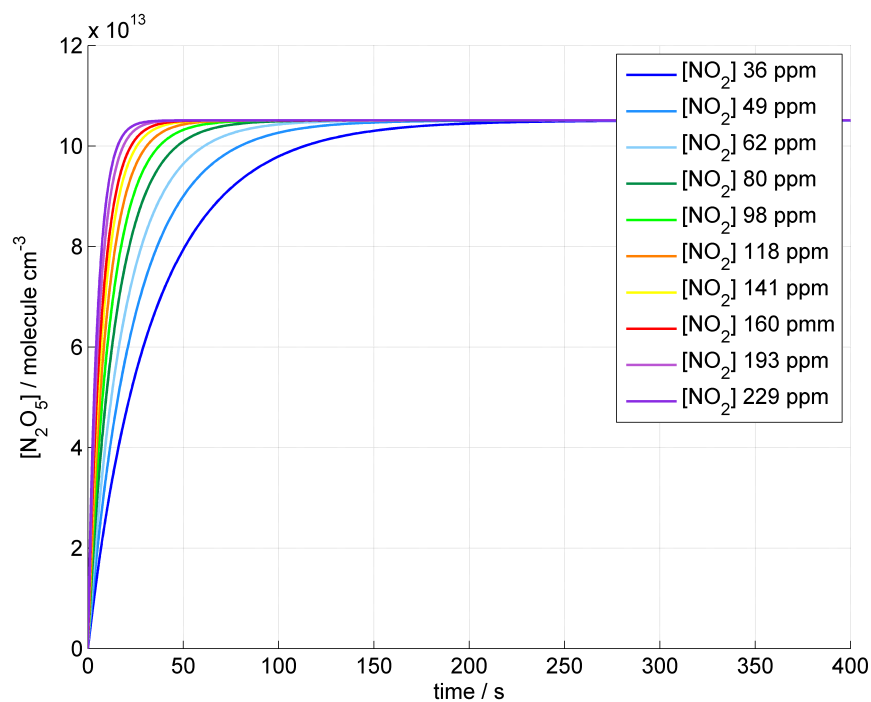
6 **Figure 8.** The formation of $[N_2O_5]$ as a function of t, calculated from Eqs 8–11 for several
7 initial values of $[NO_2]$ is shown.
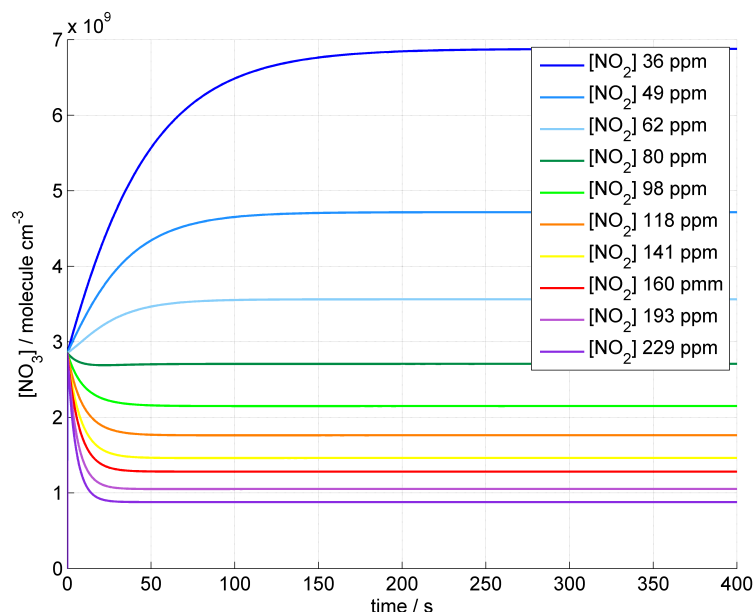
Figure 9. The formation of $[NO_3]$ as a function of t, calculated from Eqs 8–11 for several initial values of $[NO_2]$ is shown.

Since the concentrations reach constant values quickly, the data are reported just for $t \leq 400$ s. NO_2 reaches the steady state concentration faster when the initial $[NO_2]$ is higher. Ozone is totally consumed in less than 250 s (see Fig. 7). The concentration of NO_3 produced ranges from 36 ppt to 279 ppt, and it is lower when the excess of NO_2 is higher (see Fig. 9). The steady state concentrations of N_2O_5 are always approaching the same value (Fig. 8) that is determined by the initial ozone concentration.

In the experimental gas-setup a 5 dm^3 mixing bulb was used to allow the reaching of steady-state concentrations of the gas species before they entered the reaction chamber. In the NR measurements conducted at the Institut Laue-Langevin (Grenoble, France), the reaction chamber was situated in a temperature-controlled sample area while the mixing bulb was situated simply in the guide hall where the temperature was not well controlled.

An additional study of the gas system focused on the temperature dependence of the steady state concentrations to establish the impact of warm weather during the NR measurements. The rate constants (k_1, k_2 and k_3) were estimated for several temperature values and used for solving the differential Eqs 8–11. The purpose was to estimate specifically the time needed to reach a new steady state concentration due to the change in temperature between the mixing bulb in the guide hall and the reaction chamber in the sample area. For example, to calculate the steady state concentrations at $T = 30$ °C the values calculated at $T = 25$ °C were used as initial conditions for the differential equations and the solutions were computed. Fig. 10 show

1   the evolution of concentrations due to temperature increase (initial $[NO_2]$ = 36 ppm). It is

2   apparent that only a few tens of milliseconds are enough to reach the new constant

3   concentrations. (Note that the computed values for O_3 are meaningless since they are virtually

4   zero; $\approx 10^{-31}$ molecule cm^{-3}.) Evidence of this rapid establishment of equilibrium conditions

5   following a temperature change is essential information in the interpretation of the

6   experimental data recorded with NR.
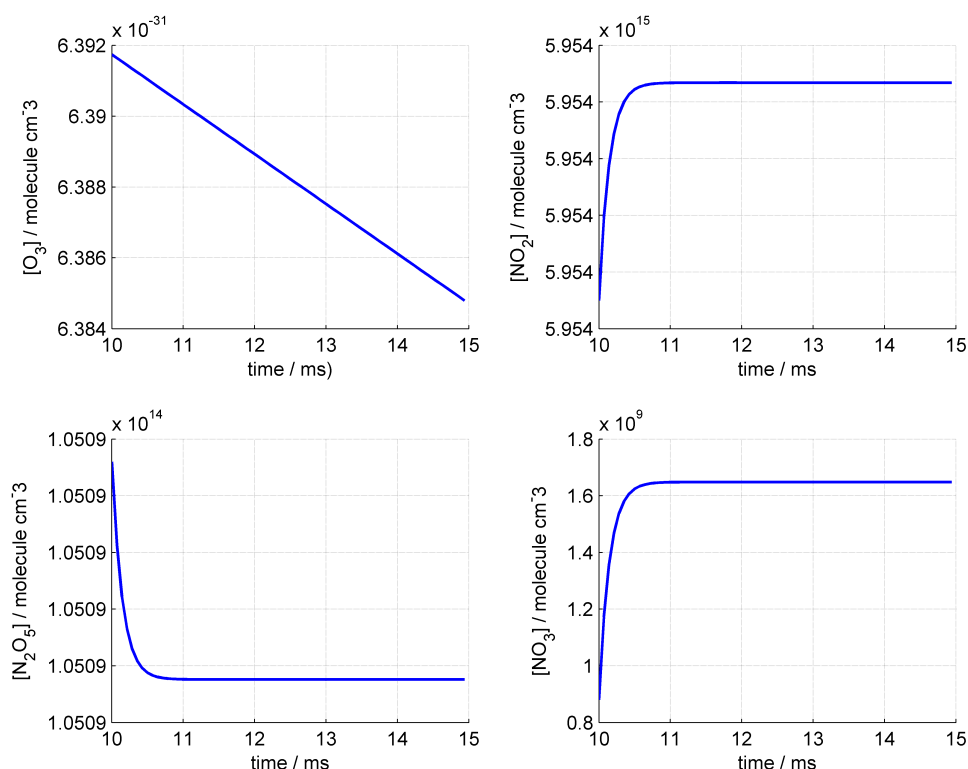
8   **Figure 10.** The evolution of the concentrations of O_3, NO_2, N_2O_5 and NO_3 due to temperature

9   increase from 25 °C to 30 °C (the initial concentration of NO_2 is 36 ppm). The equilibrium is

10 reached in tens of milliseconds.

12 The development of this model provides the means to calculate the NO_3 concentration from

13 the concentrations of NO_2 and N_2O_5. Those concentrations may be measured by IR

14 spectroscopy. Once the reactions R1 – R3 achieve the steady states the measured values for

15 $[NO_2]$ and $[N_2O_5]$ allow calculation of the $[NO_3]$ using the following equation:

16      $\frac{d[NO_3]}{dt} = 0 \implies [NO_3] = \frac{k_1[O_3][NO_2] + k_3[N_2O_5]}{k_2[NO_2]}$ (12)

17      $t \geq 400\ s, [O_3] \to 0, [NO_3] \cong \frac{k_3[N_2O_5]}{k_2[NO_2]}$ (13)

3.2 IR measurements

The measurements of the concentrations have been performed with an FTIR spectrometer (IFS/66 S, Bruker). For the very low concentrations to be detected, the most sensitive detector of the FTIR spectrometer was chosen which was a photoconductive detector (MCT D315). The acquired spectrum was averaged over 100 scans and the resolution was fixed to 1 cm^{-1}. A systematic study of the gas mixture composition as a function of [NO_2] was performed. [NO_2] in the cylinder was 1000 ppm in air, to obtain various concentrations the flow rate of NO_2 was varied from 45 cm^3 min^{-1} to 360 cm^3 min^{-1} and mixed with the carrier gas (oxygen) flowing at 1.2 dm^3 min^{-1} (the resulting concentrations are reported in Table 3).

Table 3. The flow rates of NO_3 are reported in the first column. The resulting concentrations due to mixing with O_2 flowing at 1.2 dm^3 min^{-1} are reported in the second column.

NO$_2$ flow rate / cm^3 min^{-1}	[NO$_2$] / ppm
45	36
62	49
80	62
104	80
130	98
161	118
197	141
228	160
290	193
360	229

The O_3 concentration was kept constant at 1.05×10^{14} molecule cm^{-3} by setting the oxygen flow to 1.2 dm^3 min^{-1} and the ozoniser exposure to 10 intervals, i.e. maximum UV exposure. Two types of measurements were recorded. First, in order to calculate the absorption cross section for NO_2, the mixture of O_2 and NO_2 was measured without O_3 production for each flow rate. Secondly, the spectra of the mixture produced by the reactions R1 − R3 were measured in order to record the NO_2 loss and the N_2O_5 production. For each NO_2 flow condition, at least two independent experiments were performed, in order to account for errors due to not ideal reproducibility of the experimental procedures, e.g. flow meter settings. The gas sampling chamber was a glass cylinder with a path length of 18 cm, and two circular CaF_2 windows of a diameter of 2.5 cm. The chamber inlet was connected to the exit of the 5 dm^3 mixing bulb. The outlet was connected to a bubbler. For the connections Teflon tubing and either Teflon or stainless steel gas connectors were used. The flow was admitted to the chamber for 10 minutes, then the chamber taps were closed and the chamber was disconnected from the gas flow system. Immediately after, the chamber was placed in the

sample area of the spectrometer and the measurements were recorded. Once the NO_2-O_2 mixture was measured, the glass chamber was connected again to the gas flow system and the O_2 was exposed to UV light, after 10 min, the glass chamber filled with the mixture NO_2-O_2-N_2O_5 was again put into the IR measurement area and the data were acquired. Background measurements were recorded with the chamber filled with pure oxygen.

The spectral contribution of the atmospheric gases, H_2O and CO_2, was eliminated with the atmospheric compensation routine of the FTIR instrument software. The treatment of the data has been performed with the software provided with the instrument (OPUS 5.5, Bruker). In order to obtain the absorbance due to the investigated gas species the absorbance spectrum recorded for pure oxygen was subtracted from the spectra of the mixture, then a baseline correction was performed fitting a polynomial function to the spectrum excluding the peaks. Examples of absorbance spectra is reported in Fig. 11. The spectra recorded for NO_2-O_2 are compared to the spectra of NO_2-O_2-N_2O_5 with the same initial $[NO_2]$. The characteristic peaks of NO_2 used in this study were centred at ≈ 1600 cm^{-1} and ≈ 1628 cm^{-1}.[6] A clear decrease of absorbance accounts for the NO_2 consumption due to the reactions R1 − R2. The appearance of three peaks in the spectra of NO_2-O_2-N_2O_5 can be attributed to N_2O_5 and HNO_3. The characteristic peaks used for N_2O_5 are near 1250 cm^{-1} and 1700 cm^{-1}.[7] HNO_3 absorbs close to 1320 cm^{-1} and 1710 cm^{-1}.[8,9] Initially, we did not expect to measure HNO_3, since the gas flow system was considered to be in dry conditions. The spectra show clearly the presence of HNO_3, which can be attributed to the reaction between N_2O_5 and water. For this reason, the peak at 1700 cm^{-1} has not been used to quantify N_2O_5, because it overlapped with the peak due to nitric acid. The absorbance intensity at 1250 cm^{-1} was used to obtain $[N_2O_5]$ with an absorption cross section of 1.81×10^{-18} cm^2 molecule^{-1}.[7]
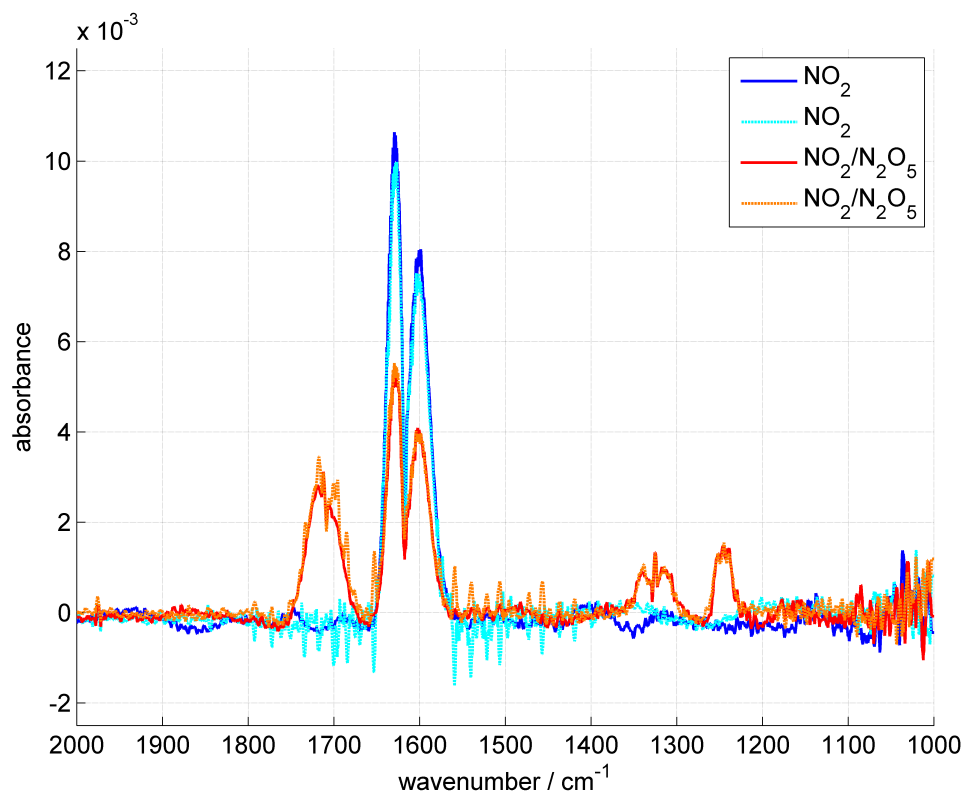
2 **Figure 11.** Absorbance spectra recorded with FTIR spectroscopy. The concentration
3 of NO_2 was 36 ppm. The blue solid line and the light blue dashed line represents the
4 spectra recorded for NO_2 carried by O_2. The red solid line and the orange dashed line
5 refer to the spectra recorded for the mixture of $NO_2 - N_2O_5$ produced by the reactions
6 R1 − R3 and carried by O_2. The background and baseline subtractions have been
7 performed using the OPUS software.
8
9 As found with the theoretical calculation, the concentration of N_2O_5 is not varying as a

10 function of the NO_2 initial concentration. The value obtained is about half of what the model

11 predicted. Since the ozone production is fairly stable and reproducible, we suggest that this

12 reduced N_2O_5 can be explained by the heterogeneous reaction of N_2O_5 with water, which is

13 rapid compared to the gas-phase reaction[3] and we found clear spectroscopic evidence of the

14 presence of HNO_3.

15 In order to calculate the NO_3 concentration, $[NO_2]$ is needed. To the best of our knowledge,

16 the absorption cross section for NO_2, ε_{NO2}, in the IR region is not available, hence we decided

17 to measure this coefficient using the mixture NO_2-O_2 and then use ε_{NO2} to quantify the

18 concentration of NO_2 after reaction. The actual concentration was derived taking into account

19 the nominal concentration of the NO_2 cylinder (1000 ppm) and the NO_2 flow rate. Figures 12

20 and 13 show the absorbance peak intensities, with and without O_3 reaction, as a function of

21 the initial NO_2 concentration.
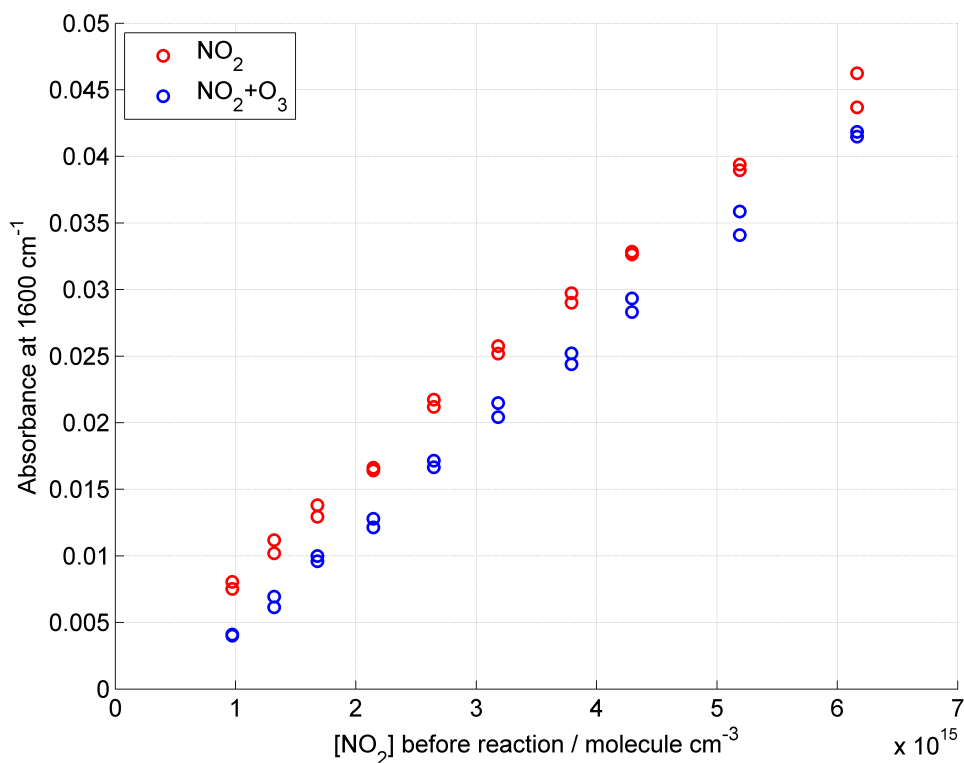
2 **Figure 12.** Intensity of the absorbance peak around 1600 cm^{-1} as a function of the
3 initial [NO$_2$]. Blue circles represent NO$_2$ mixed with O$_3$, red circles represent the NO$_2$
4 not exposed to O$_3$.
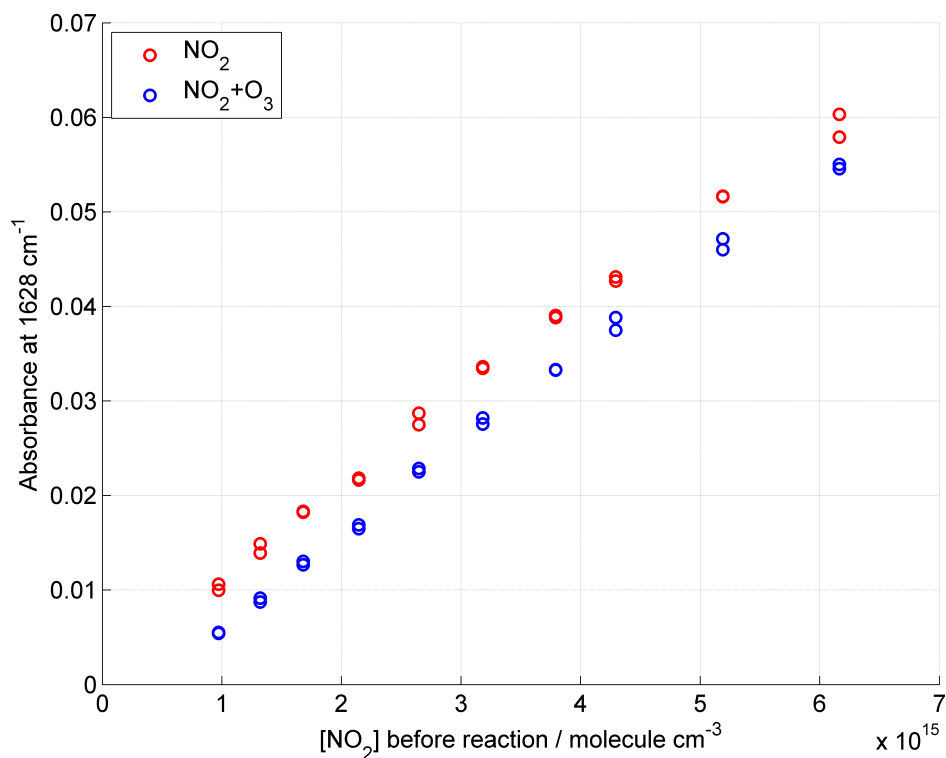
6 **Figure 13.** Intensity of the absorbance peak around 1628 cm^{-1} as a function of the
7 initial [NO$_2$]. Blue circles represent NO$_2$ mixed with O$_3$, red circles represent the NO$_2$
8 not exposed to O$_3$.
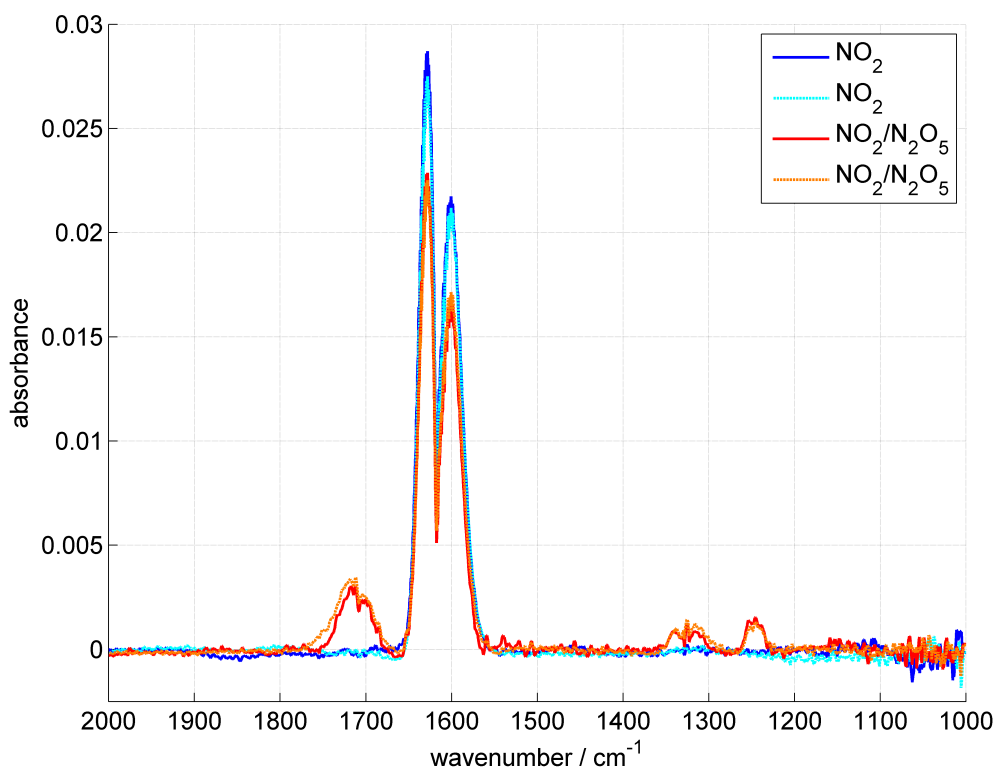
2 **Figure 14.** Absorbance spectra recorded with FTIR spectroscopy. The concentration
3 of NO$_2$ was 98 ppm. The blue solid line and the light blue dashed line represents the
4 spectra recorded for NO$_2$ carried by O$_2$. The red solid line and the orange dashed line
5 refer to the spectra recorded for the mixture of NO$_2$ − N$_2$O$_5$ produced by the reactions
6 R1 − R3 and carried by O$_2$. The background and baseline subtractions have been
7 performed using the OPUS software.
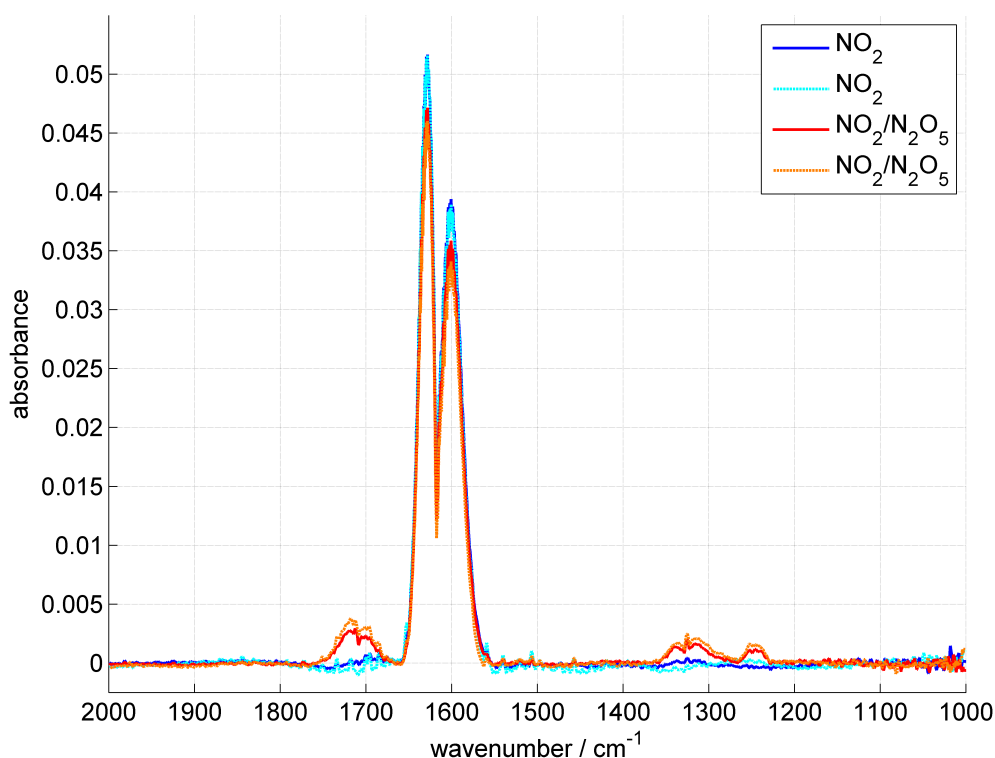
2 **Figure 15.** Absorbance spectra recorded with FTIR spectroscopy. The concentration
3 of NO2 was 193 ppm. The blue solid line and the light blue dashed line represents the
4 spectra recorded for NO2 carried by O2. The red solid line and the orange dashed line
5 refer to the spectra recorded for the mixture of NO2 − N2O5 produced by the reactions
6 R1 − R3 and carried by O2. The background and baseline subtractions have been
7 performed using the OPUS software.
8
9 The absorbance intensity increases linearly with concentration for both peaks and ε_{NO2} can be

10 calculated from the red data set. The values obtained from the linear fit to those data are: ε_{NO2}

11 $(1600 \text{ cm}^{-1}) = (4.22 \pm 0.04) \times 10^{-19} \text{ cm}^2 \text{ molecule}^{-1}$ for the peak near 1600 cm^{-1} and ε_{NO2}

12 $(1628 \text{ cm}^{-1}) = (5.57 \pm 0.05) \times 10^{-19} \text{ cm}^2 \text{ molecule}^{-1}$ for the peak near 1628 cm^{-1}.

13 The concentration of NO_2 after the reaction with ozone has been calculated using the two

14 absorption cross sections, $\varepsilon_{NO2} (1600 \text{ cm}^{-1})$ and $\varepsilon_{NO2} (1628 \text{ cm}^{-1})$. The loss of NO_2 is almost

15 constant as a function of the initial concentration. The NO_2 loss measured is about four times

16 the initial O_3 concentration, hence it is double of the value expected from the model ($\approx 2.1 \times$

17 10^{14} molecule cm^{-3}). In the model the equilibrium between NO_2 and N_2O_4 was not

18 considered, and hence this may account for the extra loss of NO_2 recorded.

19 Furthermore, other minor reactions were not taken into account in the model, such as the NO_2

20 photolysis and the heterogeneous reaction on NO_2 with liquid water.[10]

21 Even if other reactions were found to affect the final concentrations of NO_2 and N_2O_5, the

22 amount of NO_3 produced is determined by the reactions R2 − R3, which control the

1   equilibrium within the NO_2-N_2O_5-NO_3 system, hence [NO_3] can be calculated using Equation

2   13. The concentration of NO_3 is shown in Fig. 16 as a function of the initial [NO_2]. [NO_3]

3   ranges from 13 ppt to 160 ppt, which is representative for atmospheric conditions.[11] Any loss

4   of NO_3 due to reactions different from the recombination with NO_2 are not taken into account

5   for the calculation.
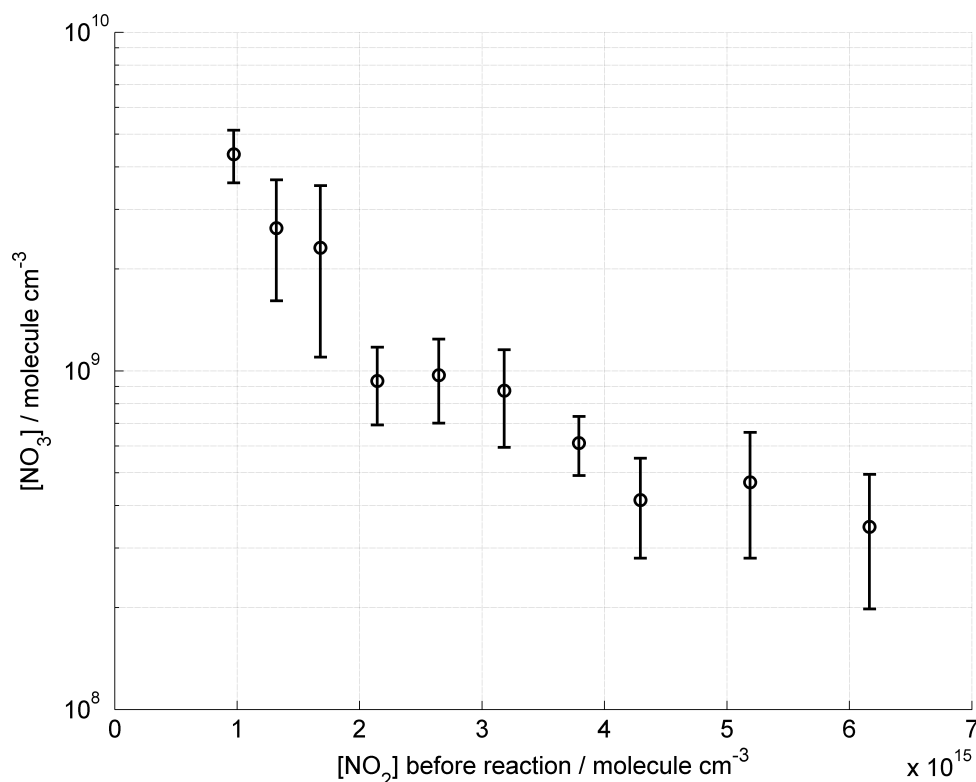
7   **Figure 16.** The concentration of NO_3 produced in reactions R1 − R3 and calculated

8   from Eq. 12 is shown as a function of the initial concentration of NO_2. As expected,

9   the NO_3 production decreases as [NO_2] increases.

11   **4. Kinetic Modelling: Model Description and Fitting Procedures**

12   **4.1 Model description: gas species**

13   In this section the description of the kinetic model is completed with all the details about the

14   processes involving the gas species: adsorption, desorption, transport and reaction.

15   From the kinetic theory, the flux of colliding X_i molecules with the surface can be expressed

16   as

17   $$J_{\text{coll},X_i} = \frac{\omega_{X_i}}{4} [X_i]_{gs} \qquad\qquad (14)$$

18   where [X_i]$_{gs}$ is the near-surface gas concentration that is assumed to be the same as the gas

19   phase concentration. As a result of the finite time required to fill the chamber, the gas-phase

20   concentration in the chamber is described as $[X_i]_{gs} = [X_i]_v\left(1 - e^{-(f/v)t}\right)$, where f is the flow

1   rate, v is the volume of the chamber and $[X_i]_v$ is the oxidant concentration measured by IR

2   spectroscopy (see Section 3 for details). ω_{NO3} is the mean thermal velocity given by

3     $\omega_{X_i} = \sqrt{8RT/\pi M_{X_i}}$, where M_{X_i} is the molar mass of X_i, R is the gas constant and T is the

4   absolute temperature. The flux of gas molecules adsorbed on the organic layer is expressed by

5     $$J_{ads,X_i} = \alpha_{s,X_i} J_{coll,X_i} \qquad (15)$$

7   where α_{s,X_i} is the surface accommodation coefficient. In the Langmuir adsorption model, α_{s,X_i}

8   is determined by the product of the surface accommodation coefficient on an adsorbate–free

9   surface, $\alpha_{s,0,X_i}$, and the sorption layer coverage θ_s which is given by the sum of the surface

10   coverage of all competing adsorbate species (*i.e.* NO_3 and NO_2).

12     $$\alpha_{s,X_i} = \alpha_{s,0,X_i}\left(1 - \sum_i \theta_{s,X_i}\right) = \alpha_{s,0,X_i}\left(1 - \sum_i \sigma_{X_i}[X_i]_s\right) \qquad (16)$$

13   The surface coverage is defined as the ratio between the actual and the maximum surface

14   concentration value of the gas species, X_i:

15     $$\theta_{s,X_i} = [X_i]_s/[X_i]_{s,max} = \sigma_{X_i}[X_i]_s \qquad (17)$$

16   The adsorbed molecule can thermally desorb back to the gas phase.

17   Desorption can be described by a first–order rate coefficient, k_{d,X_i}, which is assumed to be

18   independent of θ_{s,X_i}. The flux of desorption of gas-phase molecules can be expressed as

19     $$J_{des,X_i} = k_{d,X_i}[X_i]_s = \tau_{d,X_i}^{-1}[X_i]_s \qquad (18)$$

20   The desorption lifetime τ_{d,X_i} is the mean residence time on the surface in the absence of

21   surface reaction and surface bulk transport. For NO_3 we assume to have two desorption

22   lifetimes, $\tau_{d,NO3,1}$ and $\tau_{d,NO3,2}$, which are combined to give an effective desorption time $\tau_{d,NO3,eff}$

23   weighted by the organic surface coverage, $\theta_{ss} = [Y]_{ss}/[Y]_{ss,0}$ as

24     $$\tau_{d,NO_3,eff}^{-1} = \theta_{ss}\tau_{d,NO_3,1}^{-1} + (1 - \theta_{ss})\tau_{d,NO_3,2}^{-1} \qquad (19)$$

25   This change in desorption time is related to the change of orientation of the organic molecules

26   at the interface, *i.e.* for a highly packed monolayer the reactive site is assumed to be less

27   accessible, and the oxidant has less affinity for other parts of the molecules hence the

28   desorption is faster. When the organic surface coverage decreases the reactive sites become

29   more accessible and the desorption is slowed down. For NO_2 we considered a single

1   desorption lifetime, $\tau_{d,NO2}$. Once adsorbed to the surface, the gas-phase molecules can be

2   transported to the bulk water and vice versa. The corresponding fluxes can be expressed as

3    $J_{sb, X_i} = k_{sb,X_i}[X_i]_s$ (20)

4    $J_{bs, X_i} = k_{bs,X_i}[X_i]_b$ (21)

5   where k_{bs,X_i} in cm s^{-1} is a transport coefficient and can be regarded as effective transport

6   velocity. The bulk diffusion coefficient, D_{b,X_i}, can be used to estimate this transport velocity,

7    $k_{bs,X_i} \approx 4D_{b,X_i}/\pi\lambda_{X_i}$ where λ_{X_i} is the average travel distance from the near-surface bulk into

8   the sorption layer. To estimate k_{sb,X_i} the rate coefficients for gas–surface and surface–bulk

9   transport can be matched with a literature value or estimate for the Henry's law coefficient or

10   gas–particle equilibrium partitioning coefficient (H_{X_i}):

12   $k_{sb,X_i} = \dfrac{4k_{bs,X_i}H_{X_i}}{\alpha_{s,X_i}\tau_{d, X_i}\omega_{X_i}}$ (22)

4.2 Fitting: choice of free and fixed parameters

14   The kinetic model depends on several parameters, and some of them are strongly correlated.

15   For example, for a given gas species time evolution, which may be described by certain

16   accommodation coefficients ($\alpha_{s,0,X_i}$ where X_i is NO_3 or NO_2) and certain desorption lifetimes

17   (τ_{d, X_i}), a good fit may be obtained as well with a lower $\alpha_{s,0,X_i}$ and an higher τ_{d,X_i}. The

18   accommodation coefficient represents the probability of the gas-phase molecule to absorb at

19   the organic layer, hence the lower $\alpha_{s,0,NO3}$ is, the smaller is the probability of the reaction with

20   the organic molecule. The desorption lifetime represents the mean residence time of the

21   molecule absorbed at the surface, hence the longer the time is, the higher is the probability for

22   the gas molecule to react (valid for NO_3). NO_2 does not react with the organic layer,[12] but

23   those parameters still compensate, because $\alpha_{s,0,NO2}$ determines the number of molecules

24   absorbed and $\tau_{d,NO2}$ determines the number of molecules leaving the sorption sites. The choice

25   of leaving both of these parameters free to vary in the fitting will lead to a wide range of

26   values for both. The resulting surface excess will match the experimental data. However, the

27   choice of fixing one out of these two parameters makes the optimisation of the model

28   computationally easier and the comparison between different organic molecules possible.

4.3 Fitting Results

4.3.1 dOA exposed to NO_3
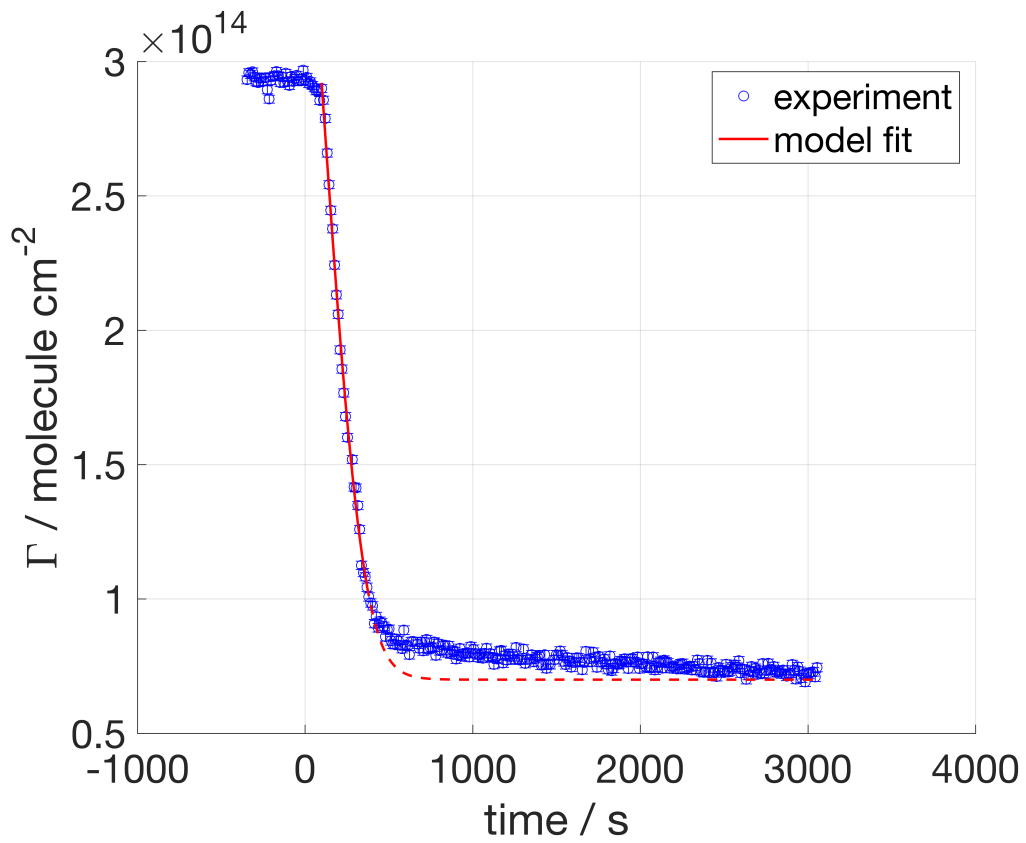
2 **Figure 17.** dOA exposed to 86 ppt NO₃.
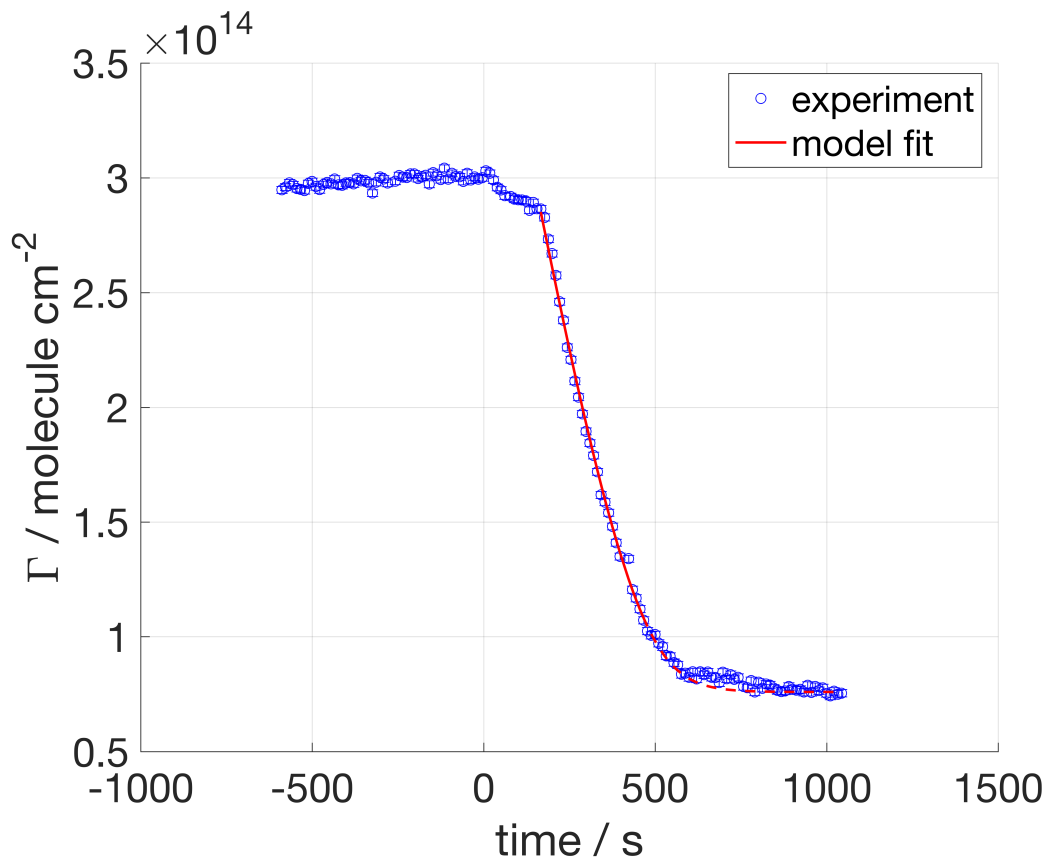
5
6 **Figure 18.** dOA exposed to 86 ppt NO₃.
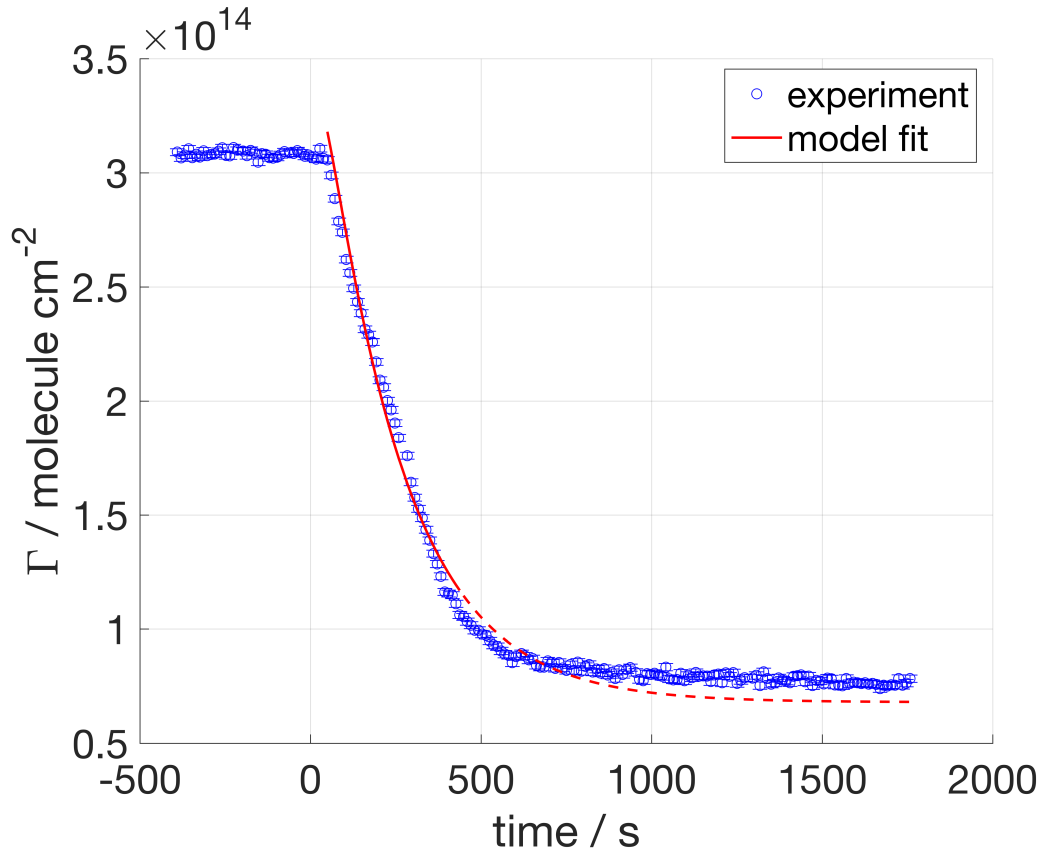
4   **Figure 19.** dOA exposed to 35 ppt NO₃.
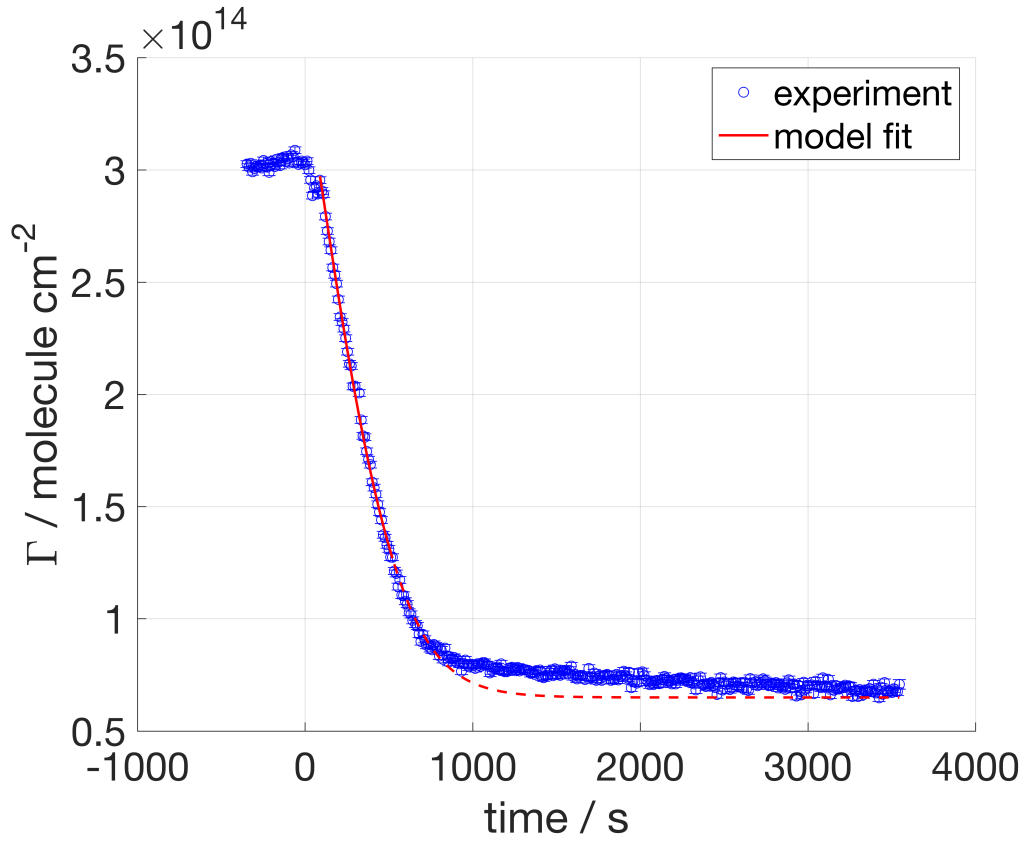
6   **Figure 20.** dOA exposed to 36 ppt NO₃.
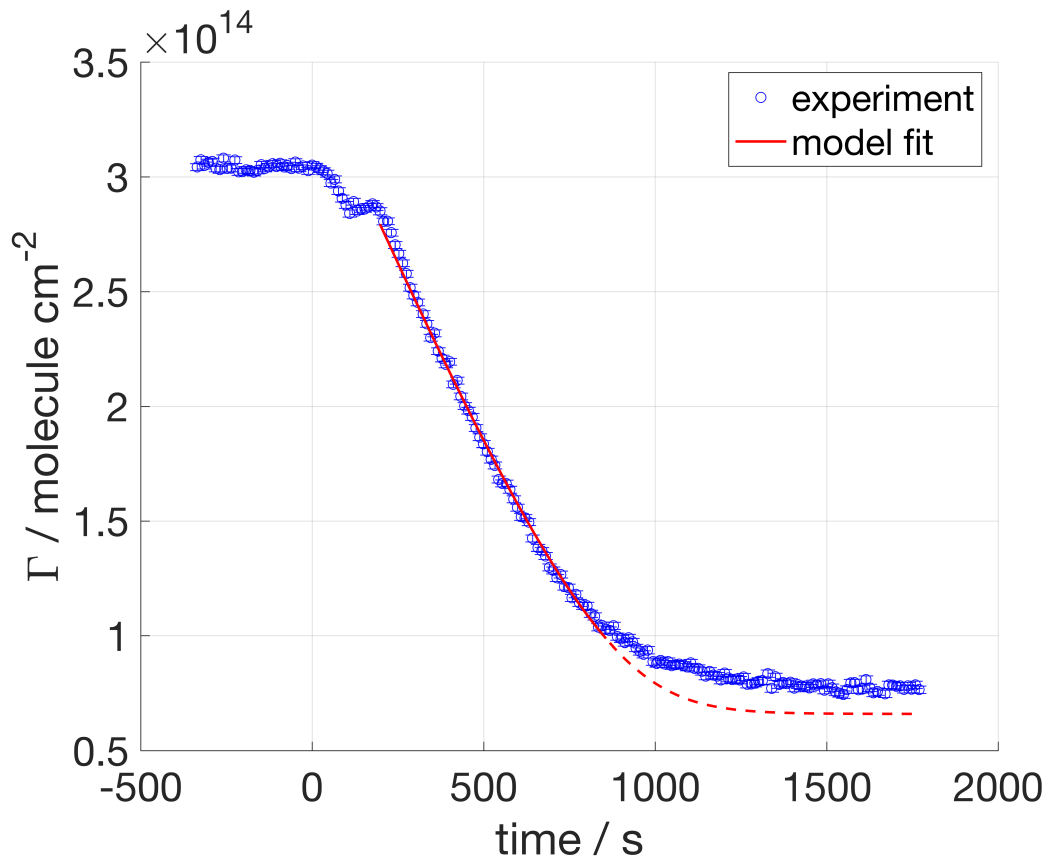
3 **Figure 21.** dOA exposed to 36 ppt NO_3.
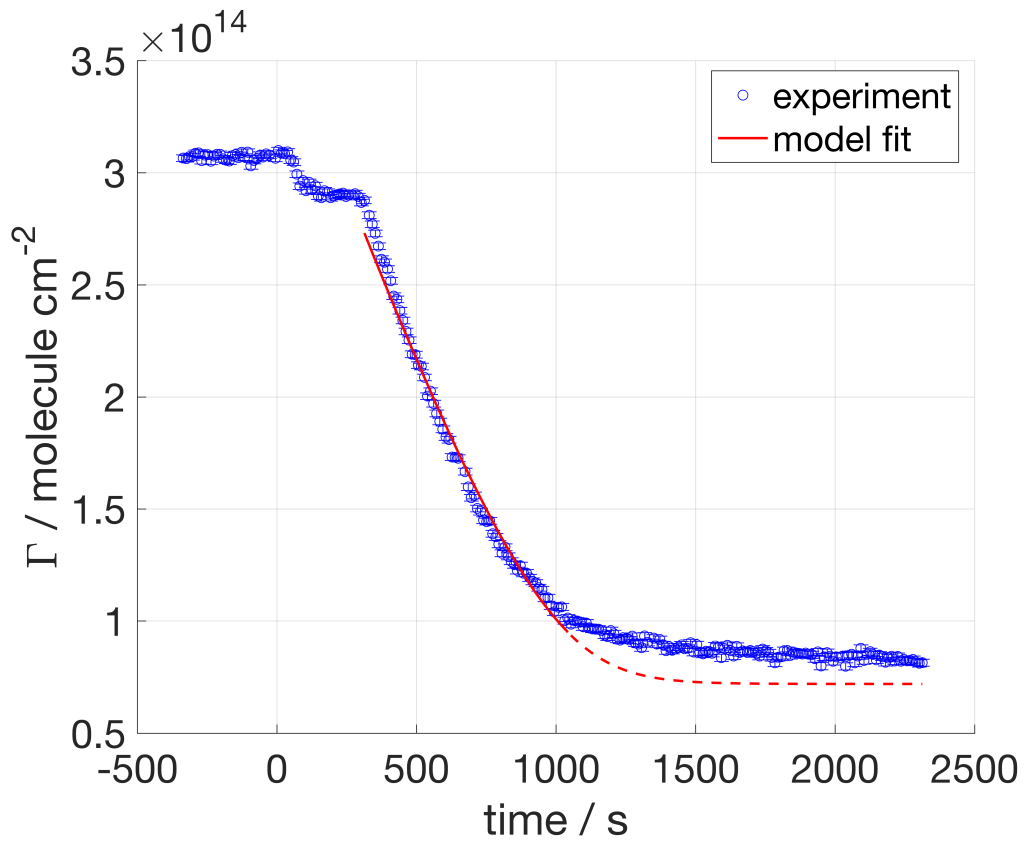
6 **Figure 22.** dOA exposed to 32 ppt NO_3.
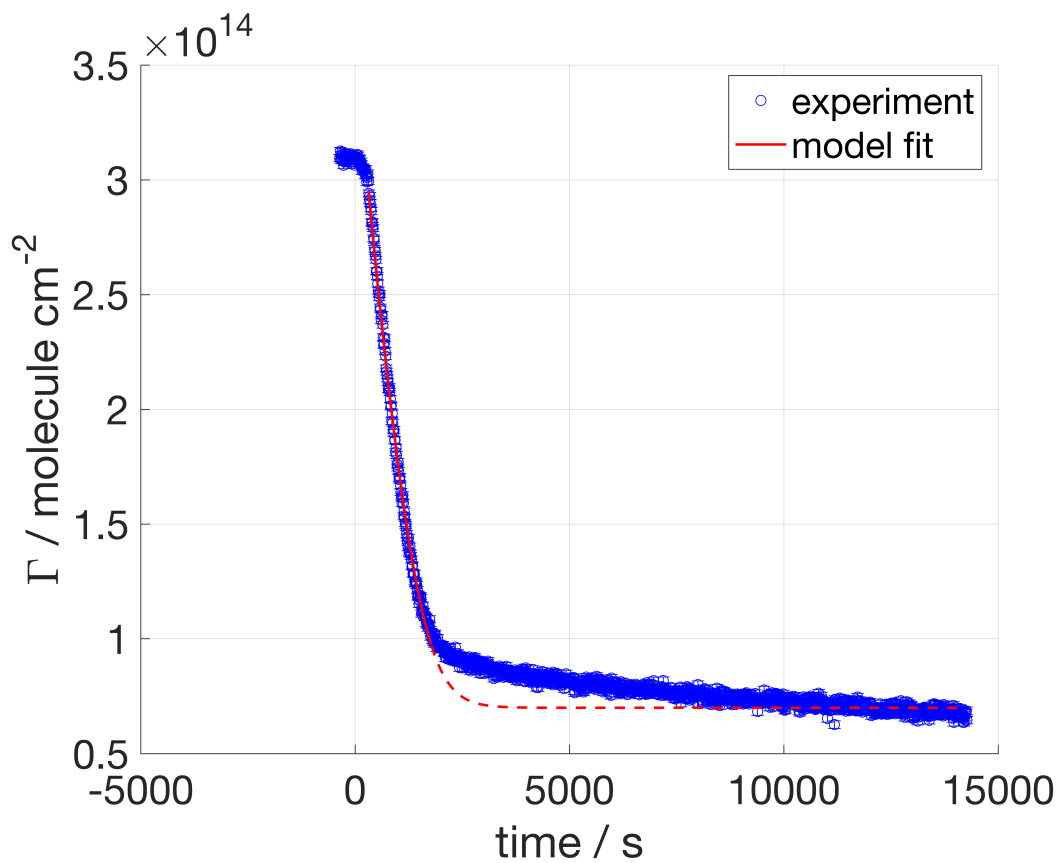
2 **Figure 23.** dOA exposed to 15 ppt NO$_3$.
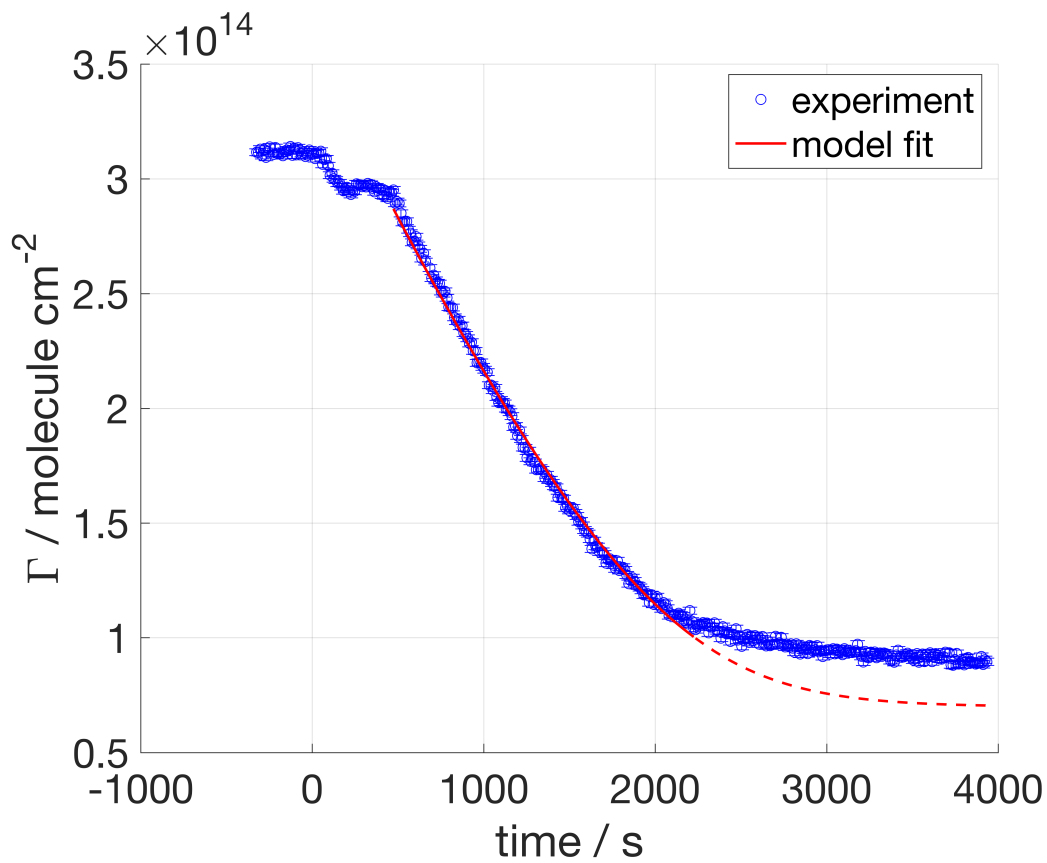
5 **Figure 24.** dOA exposed to 15 ppt NO$_3$.
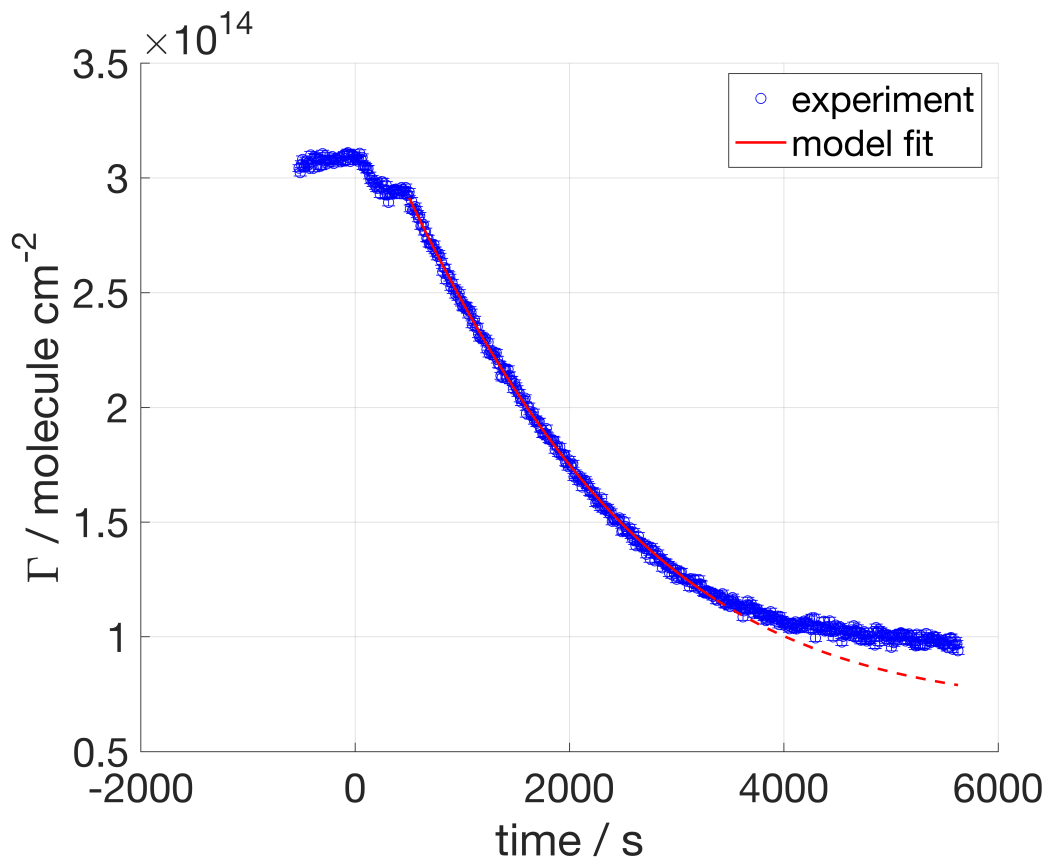
2 **Figure 25.** dOA exposed to 13 ppt NO₃.
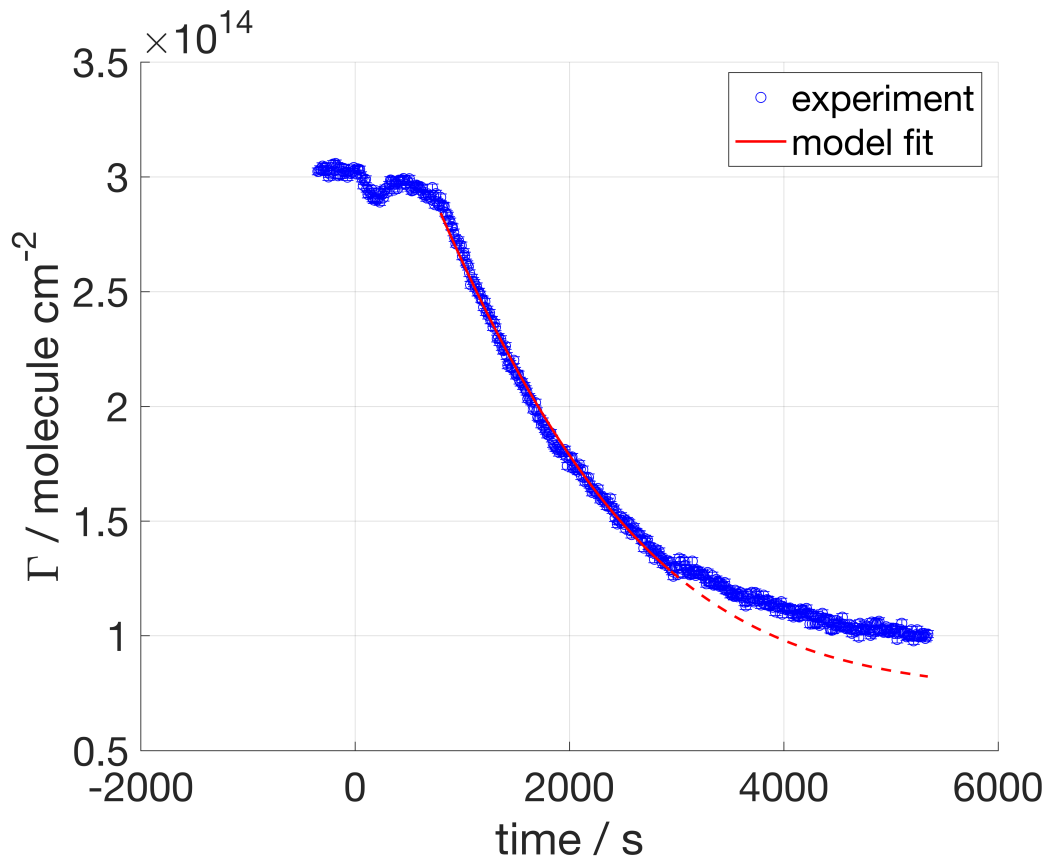
5 **Figure 26.** dOA exposed to 13 ppt NO₃.

2 **4.3.2 dPOA exposed to NO₃**
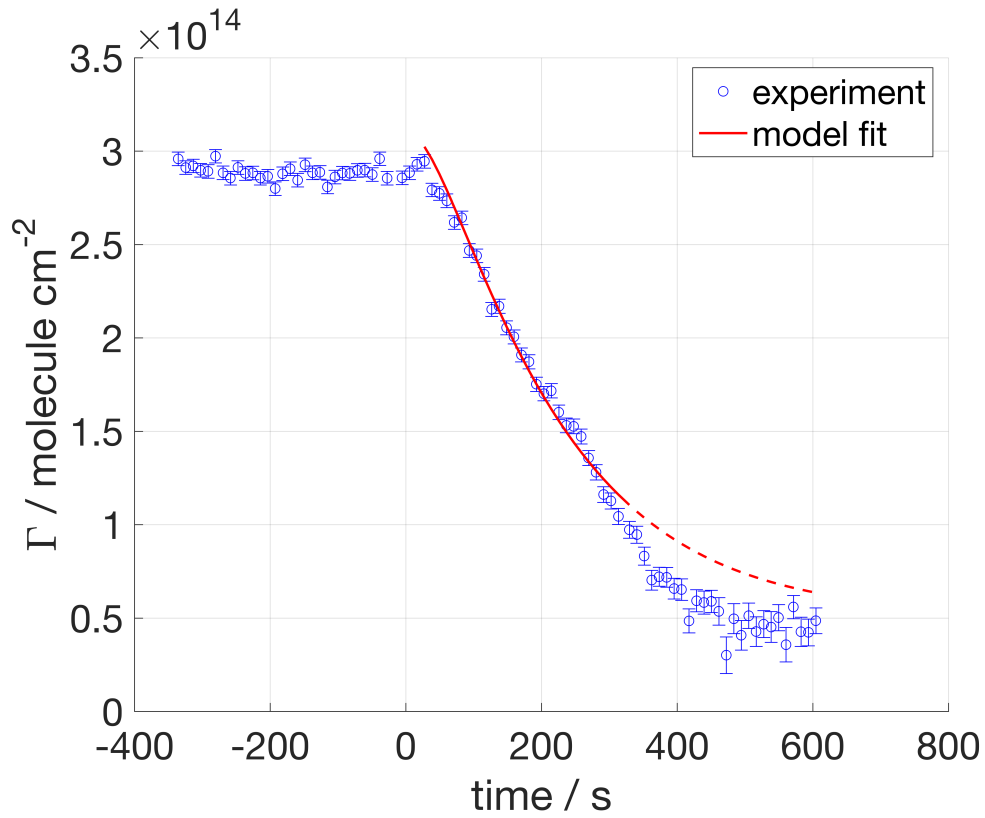
4 **Figure 27.** dPOA exposed to 86 ppt NO₃.
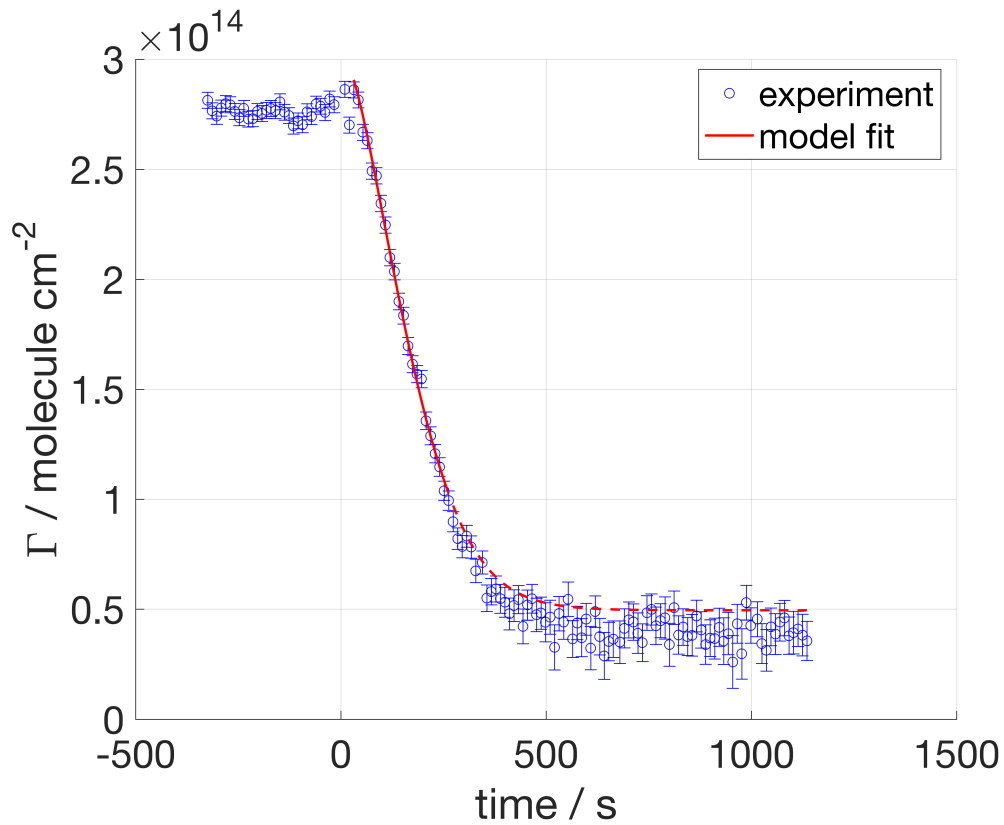
7 **Figure 28.** dPOA exposed to 86 ppt NO₃.
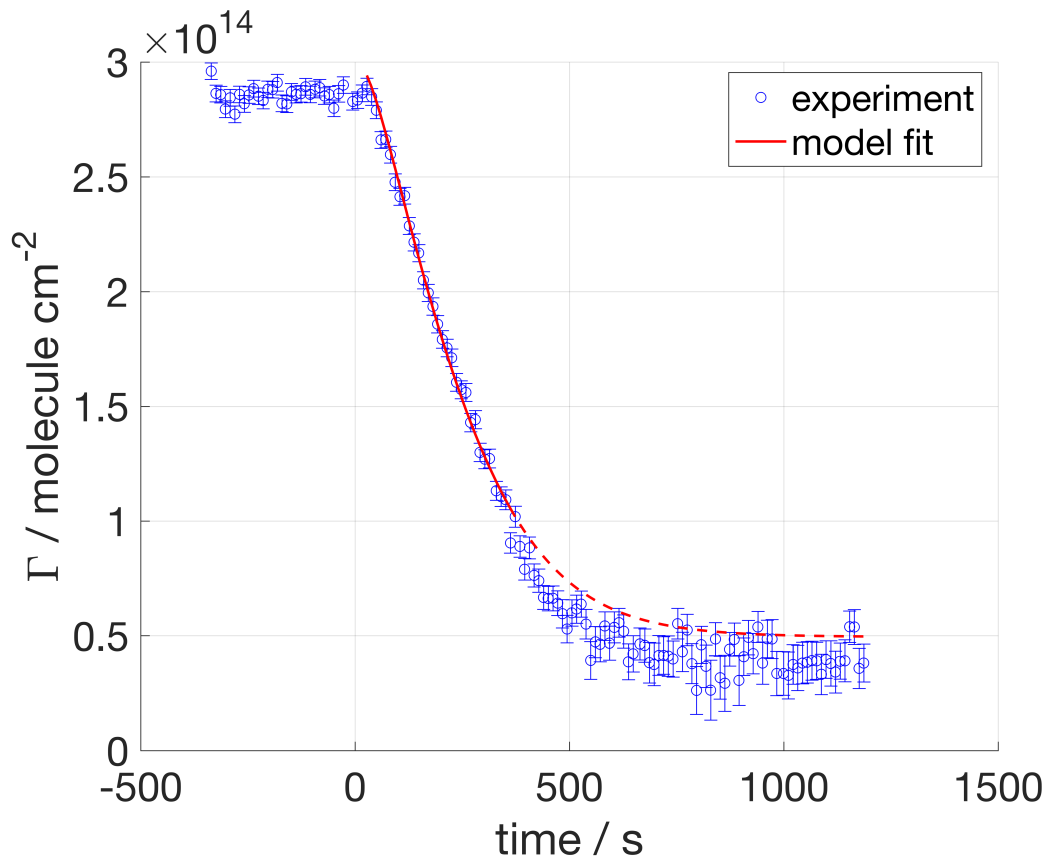
3   **Figure 29.** dPOA exposed to 35 ppt NO₃.
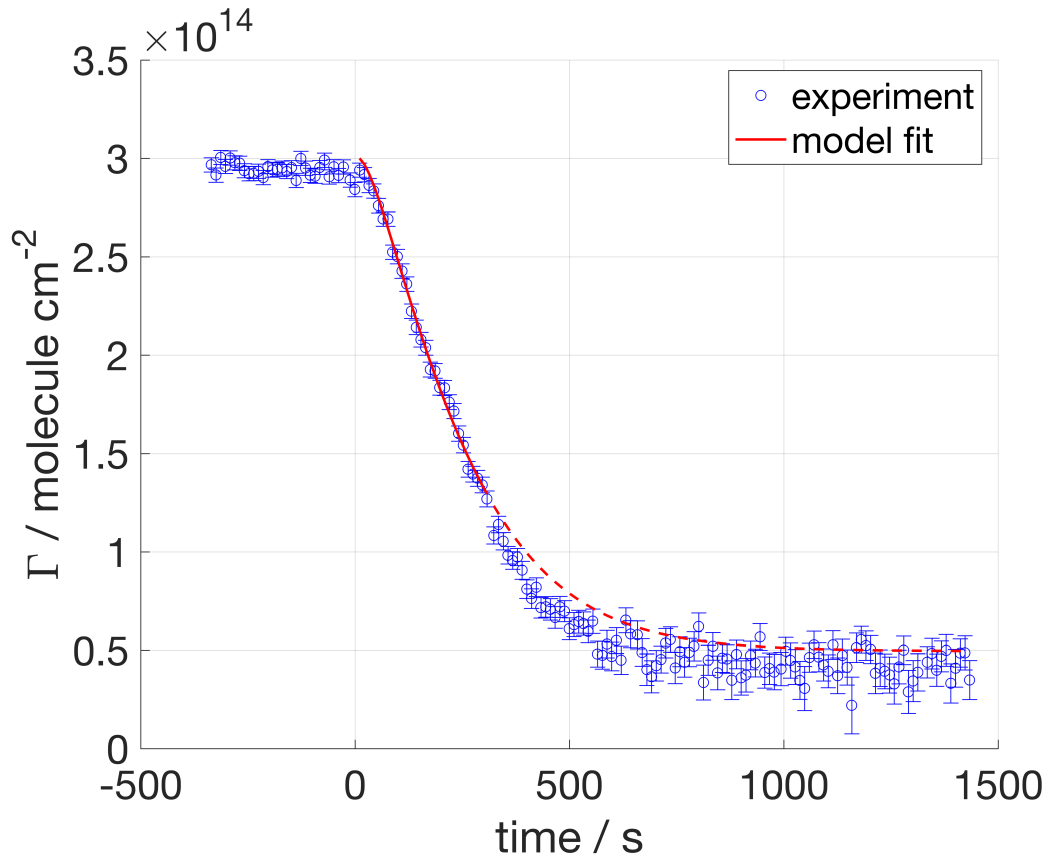
5   **Figure 30.** dPOA exposed to 36 ppt NO₃.
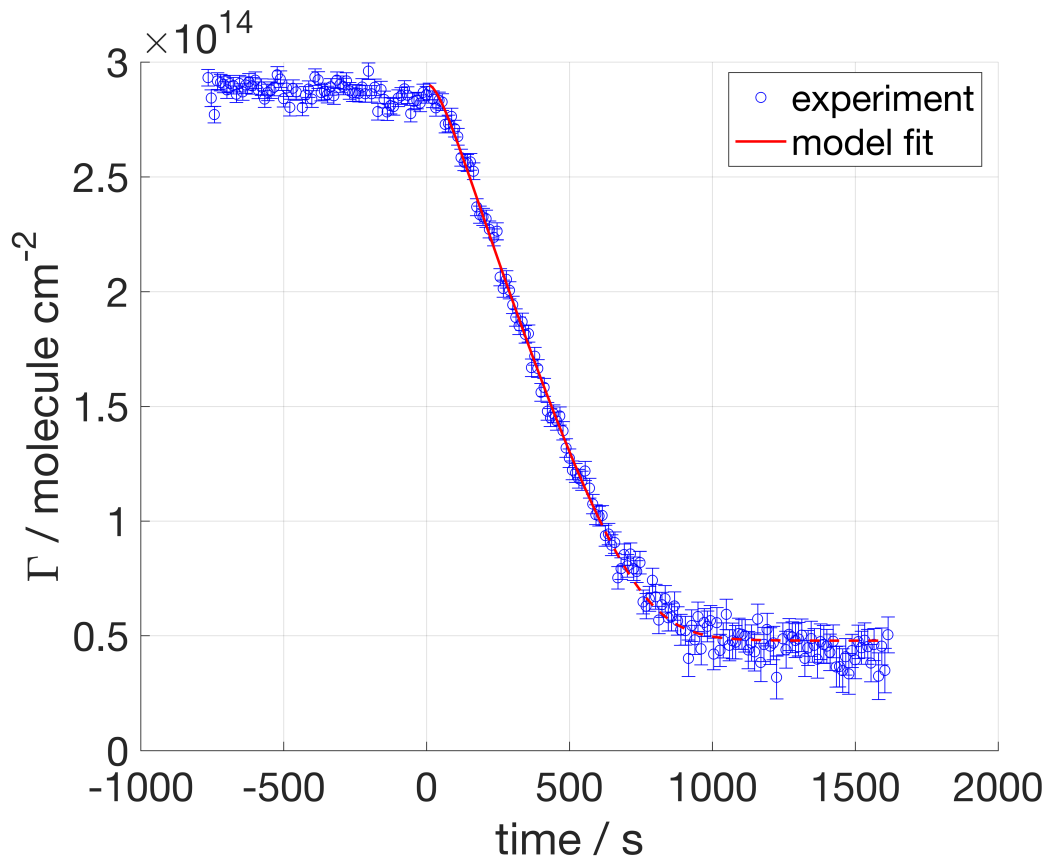
Figure 31. dPOA exposed to 32 ppt NO₃.
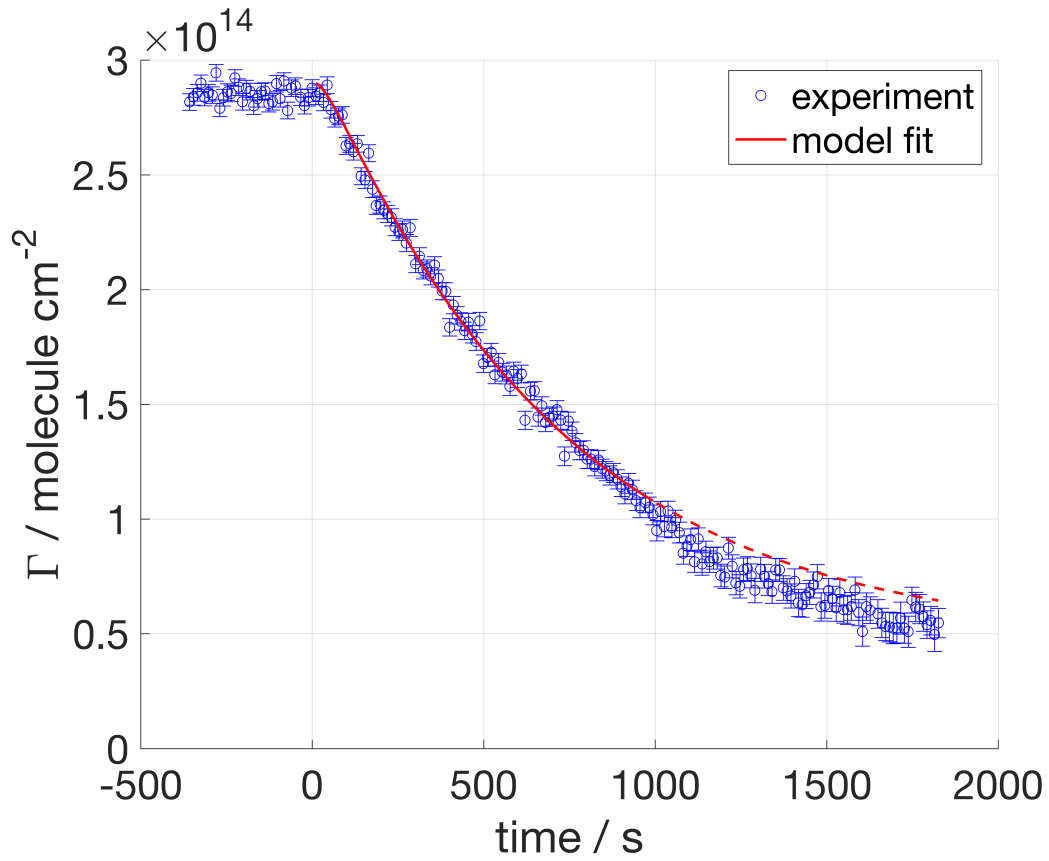
Figure 32. dPOA exposed to 15 ppt NO₃.
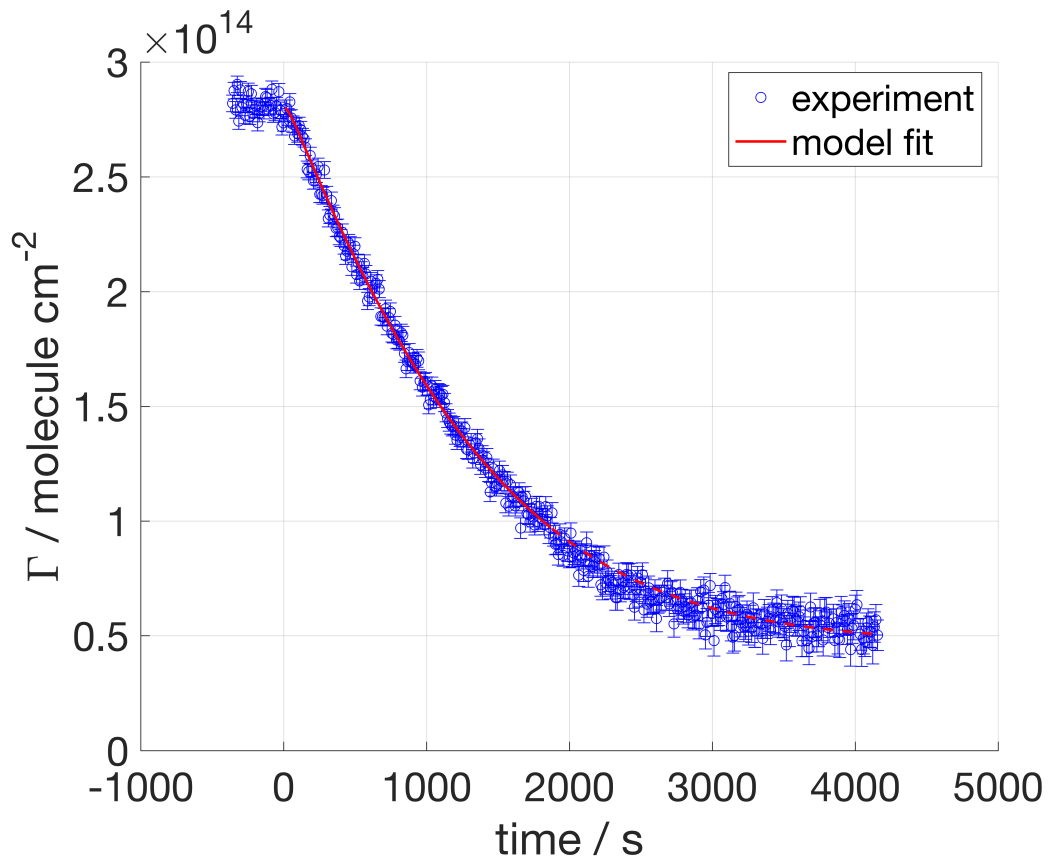
3 **Figure 33.** dPOA exposed to 13 ppt NO_3.
4
5 **4.3.3 dMO exposed to NO_3**
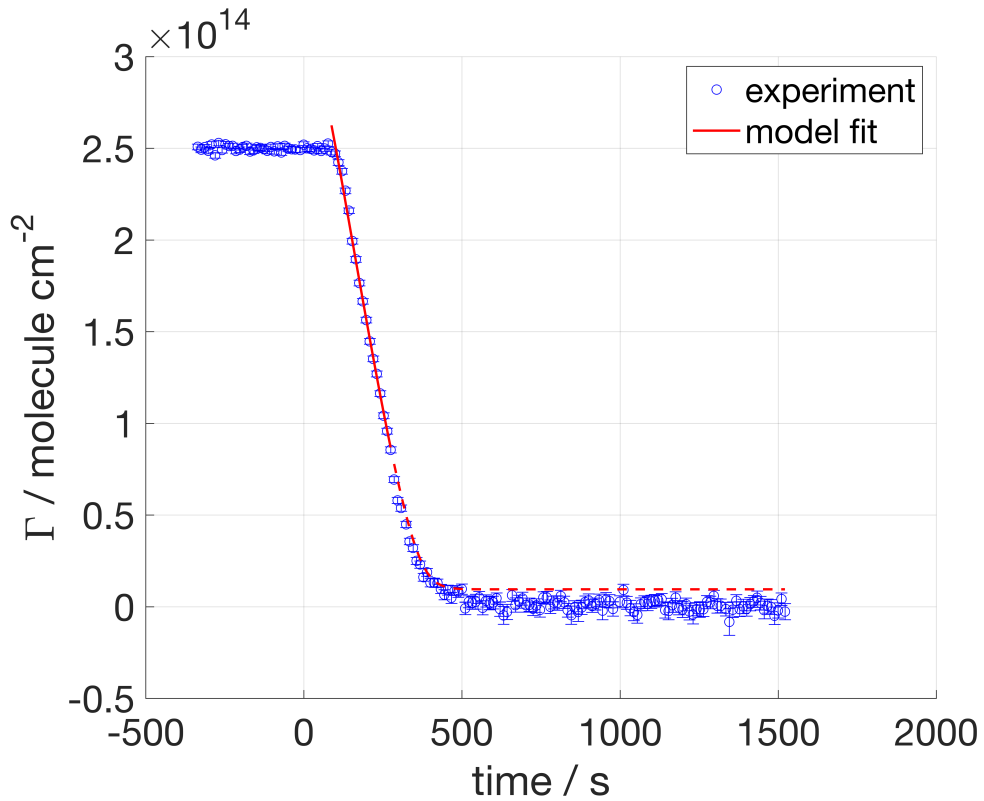
7 **Figure 34.** dMO exposed to 86 ppt NO_3.
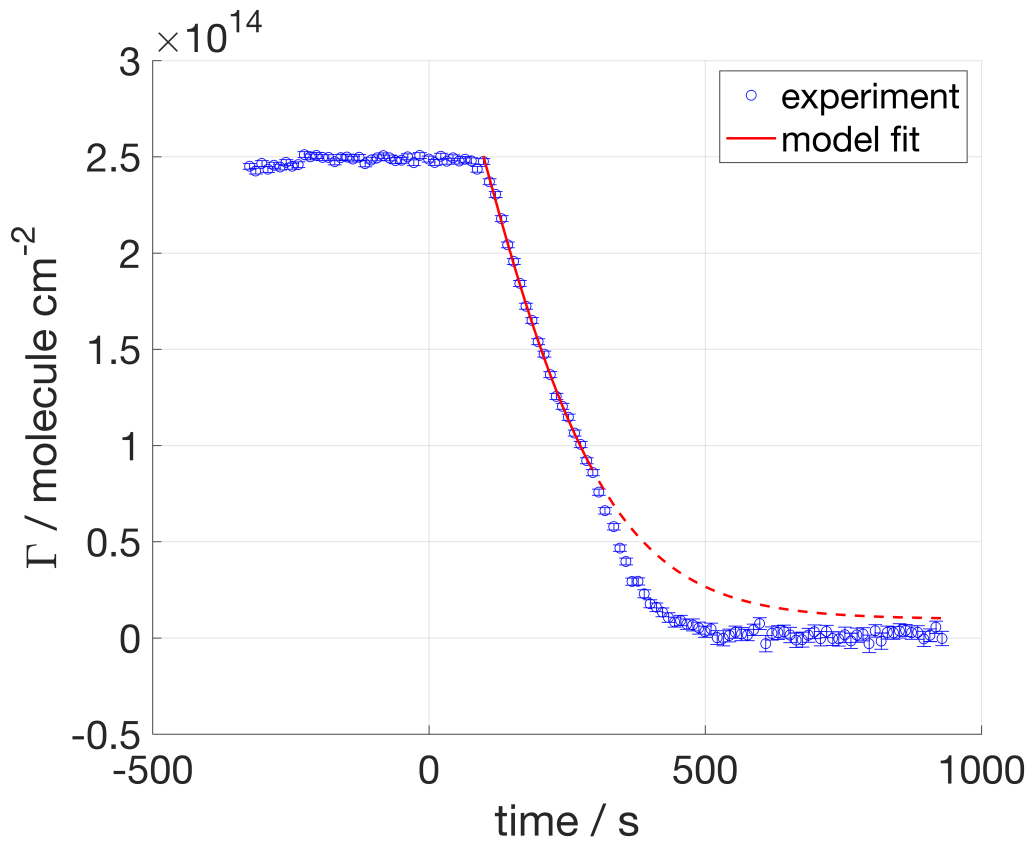
3 **Figure 35.** dMO exposed to 86 ppt NO$_3$.
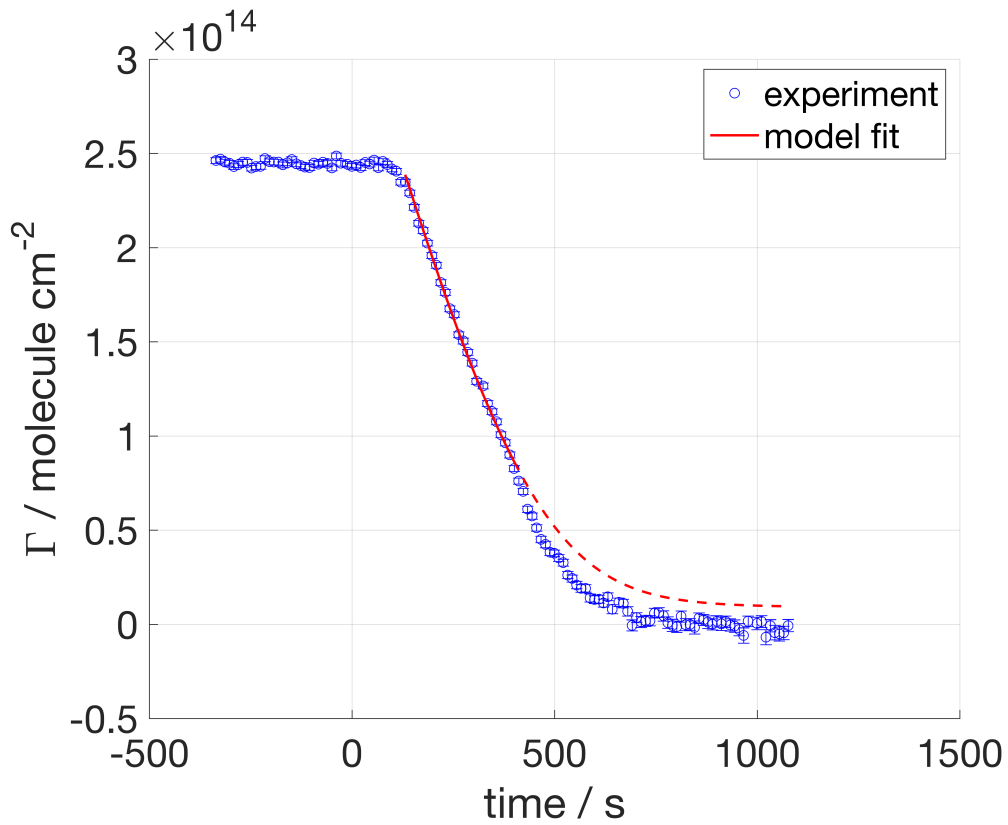
6 **Figure 36.** dMO exposed to 36 ppt NO$_3$.
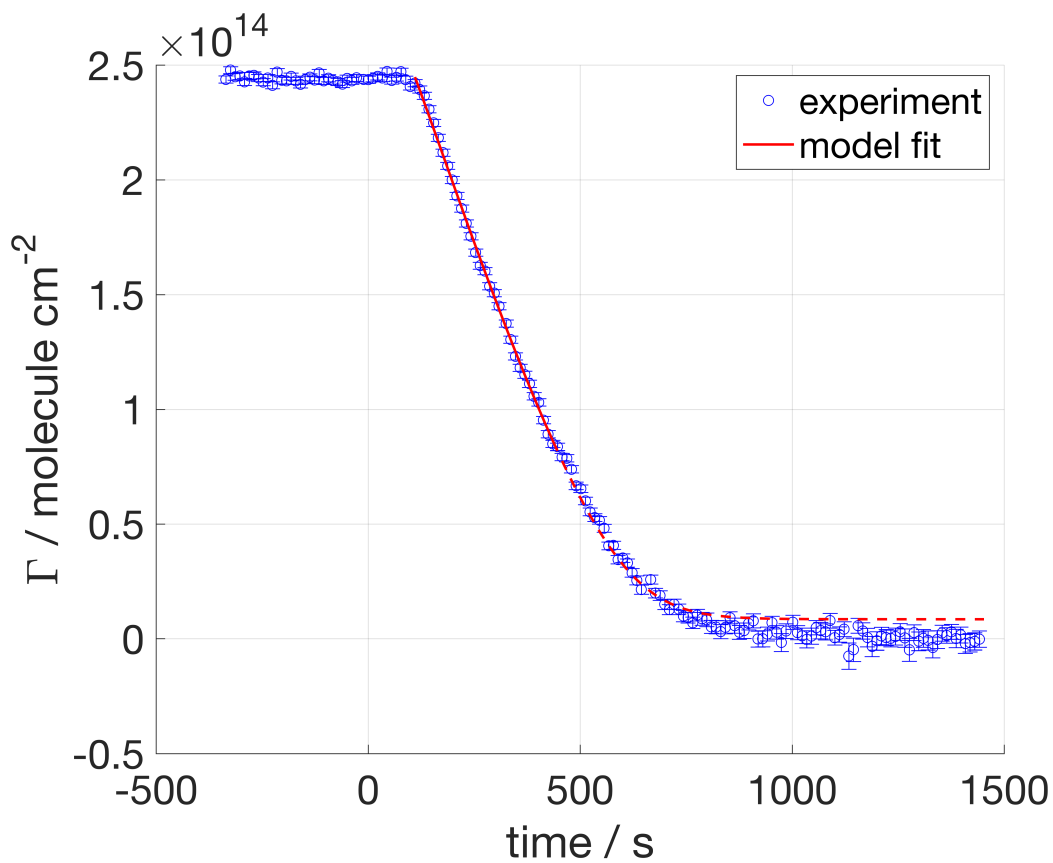
2 **Figure 37.** dMO exposed to 36 ppt NO$_3$.
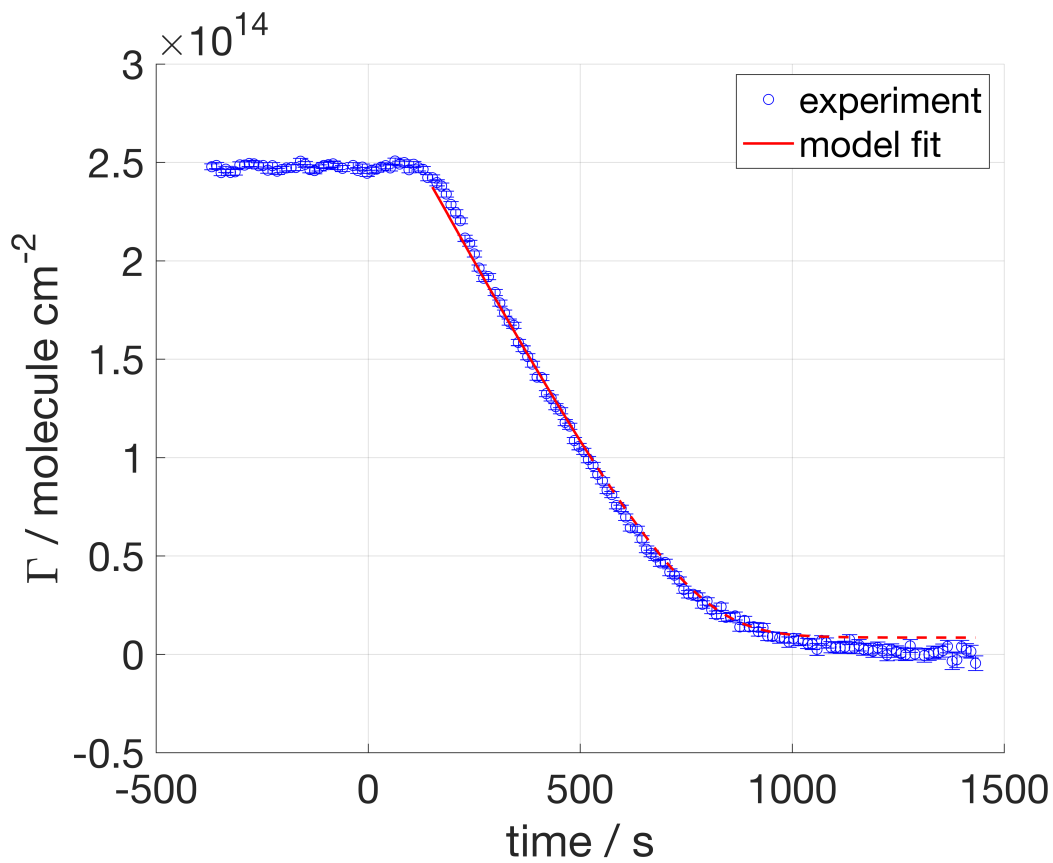
5 **Figure 38.** dMO exposed to 32 ppt NO$_3$.
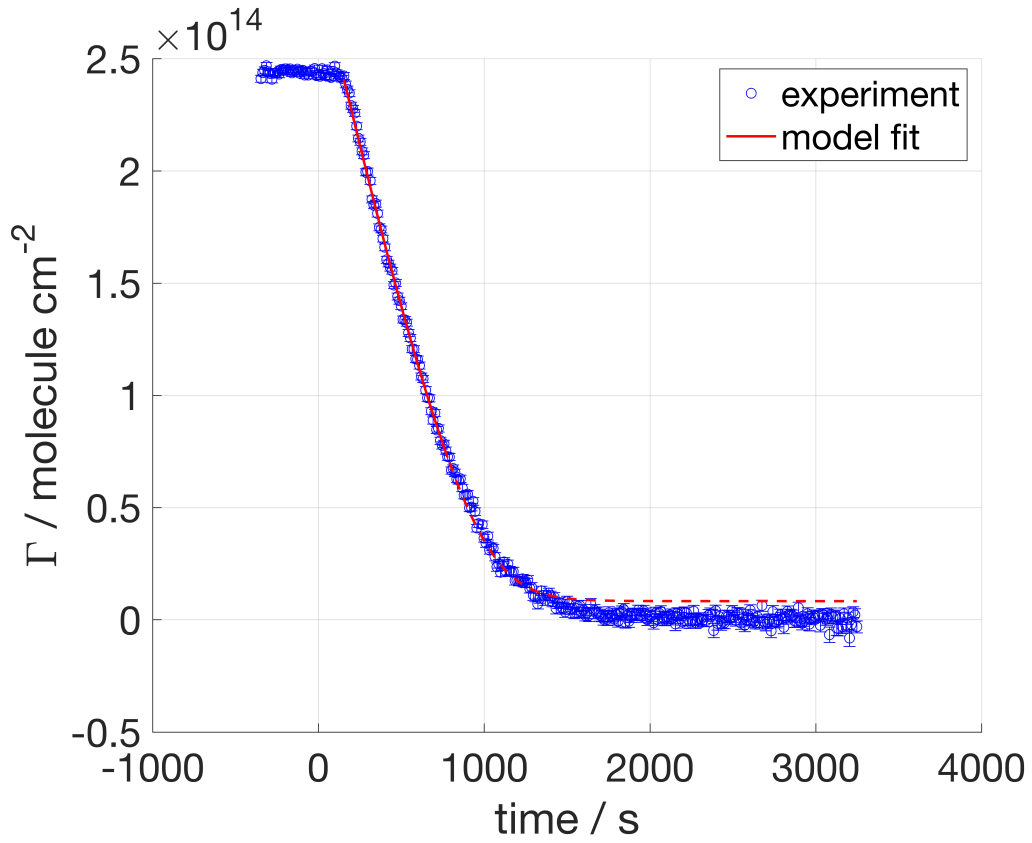
2 **Figure 39.** dMO exposed to 15 ppt NO₃.
3
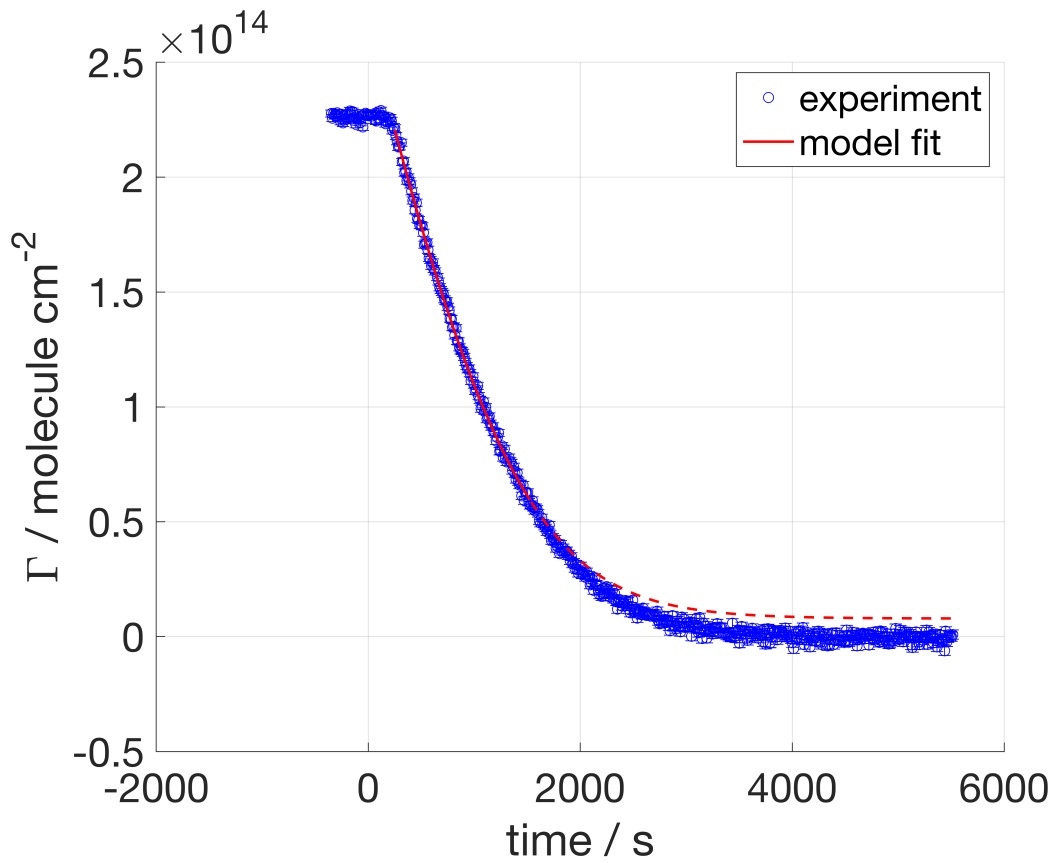
6 **Figure 40.** dMO exposed to 13 ppt NO₃.

References

1. Barnes, G. & Gentle, I. *Interfacial science: an introduction.* (Oxford University Press, 2010).

2. Sander, S. P. *et al.* Chemical Kinetics and Photochemical Data for Use in Atmospheric Studies, Evaluation No. 17. *JPL Publ. 10-6* (2011).

3. Seinfeld, J. H. & Pandis, S. N. *Atmospheric Chemistry and Physics: From Air Pollution to Climate Change.* (John Wiley & Sons, Inc., 2006).

4. Troe, J. Specific rate constant k(E,J) for unimolecolar bond fission. *J. Chem. Phys.* **79,** 6017–6029 (1983).

5. MATLAB. *version 7.12.0 (R2011a).* (The Math Works Inc., 2011).

6. Guttman, A. Absolute infrared intensity measurements on nitrogen dioxide and dinitrogen tetroxide. *J. Quant. Spectrosc. Radiat. Transf.* **2,** 1–15 (1961).

7. Cantrell, C. A., Davidson, J. A., McDaniel, A. H., Shetter, R. E. & Calvert, J. G. Infrared absorption cross sections for N_2O_5. *Chem. Phys. Lett.* **148,** 358–363 (1988).

8. Hjorth, J., Ottobrini, G., Cappellani, F. & Restelli, G. A Fourier transform infrared study of the rate constant of the homogeneous gas-phase reaction nitrogen oxide (N_2O_5) + water and determination of absolute infrared band intensities of N_2O_5 and nitric acid. *J. Phys. Chem.* **91,** 1565–1568 (1987).

9. Chackerian, C., Sharpe, S. W. & Blake, T. A. Anhydrous nitric acid integrated absorption cross sections: 820-5300 cm^{-1}. *J. Quant. Spectrosc. Radiat. Transf.* **82,** 429–441 (2003).

10. Ammann, M. *et al.* Evaluated kinetic and photochemical data for atmospheric chemistry: Volume VI - heterogeneous reactions with liquid substrates. *Atmos. Chem. Phys.* **13,** 8045–8228 (2013).

11. Brown, S. S. & Stutz, J. Nighttime radical observations and chemistry. *Chem. Soc. Rev.* **41,** 6405–6447 (2012).

12. King, M. D., Rennie, A. R., Pfrang, C., Hughes, A. V & Thompson, K. C. Interaction of nitrogen dioxide (NO_2) with a monolayer of oleic acid at the air–water interface – A simple proxy for atmospheric aerosol. *Atmos. Environ.* **44,** 1822–1825 (2010).